Best Available
Copy
for all Pictures

AD/A-004 045

A STUDY OF THE DIELECTRIC BREAKDOWN OF SiO_2 FILMS ON Si BY THE SELF-QUENCHING TECHNIQUE

D. Y. Yang, et al

Princeton University

Prepared for:

Air Force Cambridge Research Laboratories
Advanced Research Projects Agency

October 1974

DISTRIBUTED BY:

NTIS

National Technical Information Service
U. S. DEPARTMENT OF COMMERCE

Unclassified

SECURITY CLASSIFICATION OF THIS PAGE (When Data Entered)

REPORT DOCUMENTATION PAGE

READ INSTRUCTIONS BEFORE COMPLETING FORM

1. REPORT NUMBER: AFCRL-TR-74-0516
2. GOVT ACCESSION NO.:
3. RECIPIENT'S CATALOG NUMBER: AD/A-004045

4. TITLE (and Subtitle): A STUDY OF THE DIELECTRIC BREAKDOWN OF SiO_2 FILMS ON Si BY THE SELF-QUENCHING TECHNIQUE

5. TYPE OF REPORT & PERIOD COVERED: Special Report No. 4

6. PERFORMING ORG. REPORT NUMBER: SPECIAL REPORT NO. 4

7. AUTHOR(s):
D. Y. Yang
Walter C. Johnson
Murray A. Lampert

8. CONTRACT OR GRANT NUMBER(s): F19628-72-C-0298

9. PERFORMING ORGANIZATION NAME AND ADDRESS:
Princeton University
Department of Electrical Engineering
Princeton, New Jersey 08540

10. PROGRAM ELEMENT, PROJECT, TASK AREA & WORK UNIT NUMBERS:
Project No. 2180
DoD Element 61101D

11. CONTROLLING OFFICE NAME AND ADDRESS:
Air Force Cambridge Research Laboratories
Hanscom AFB, Massachusetts 01731
Contract Monitor: John C. Garth/LQR

12. REPORT DATE: October 1974

13. NUMBER OF PAGES: 95

14. MONITORING AGENCY NAME & ADDRESS (if different from Controlling Office):

15. SECURITY CLASS. (of this report): Unclassified

15a. DECLASSIFICATION/DOWNGRADING SCHEDULE:

16. DISTRIBUTION STATEMENT (of this Report)

A - Approved for public release; distribution unlimited

17. DISTRIBUTION STATEMENT (of the abstract entered in Block 20, if different from Report)

Reproduced by
NATIONAL TECHNICAL
INFORMATION SERVICE
U S Department of Commerce
Springfield VA 22151

18. SUPPLEMENTARY NOTES

This research was supported by the Defense Advanced Research Projects Agency. ARPA Order No. 2180.

19. KEY WORDS (Continue on reverse side if necessary and identify by block number)

Dielectric breakdown
Silicon dioxide
Self-quenching technique

20. ABSTRACT (Continue on reverse side if necessary and identify by block number)

We have studied the dielectric breakdown of thermally grown SiO_2 films on Si substrates by the technique in which a thin metallization is used to provide self-quenching of the breakdown. Each of the four possible combinations of p or n substrate and + or - field-plate polarity shows its own distinctive properties and its own distinctive configuration of breakdown damage as viewed by optical microscope and scanning electron microscope. Some properties correlate with the nature of the substrate surface channel (inversion versus accumulation); other properties correlate with the field-plate polarity.

DD FORM 1 JAN 73 1473 EDITION OF 1 NOV 65 IS OBSOLETE

Unclassified

SECURITY CLASSIFICATION OF THIS PAGE (When Data Entered)

20. The time evolution of the breakdown indicates that the current through the fault is limited by the spreading resistance of the substrate. The combination of p substrate with positive field-plate polarity produces a breakdown configuration with four-fold symmetry (square or four-pointed star) which is related to the anisotropy of hot-electron conduction on the (100) face of the silicon substrate.

A study of the currents and insulator charging at the onset of breakdown indicates that initiation of breakdown is by Fowler-Nordheim tunneling of electrons into the oxide. The occurrence of a current instability which can be enhanced by lowering the temperature indicates the possible importance of hole-electron pair production in the oxide with subsequent trapping of holes.

ii a

ARPA Order No. 2180

Program Code No. 4D10

Contractor: Princeton University

Effective date of contract: 1 July 1972

Contract No. F19628-72-C-0298

Principal Investigator and phone no.
Prof. Walter C. Johnson/609-452-4621

AFCRL Project Scientist and phone no.
Dr. John C. Garth/617-861-4051

Contract expiration date: 30 June 1975

Qualified requestors may obtain additional copies from the Defense Documentation Center. All others should apply to the National Technical Information Service.

TABLE OF CONTENTS

CHAPTER I
INTRODUCTION

Dielectric breakdown is defined here as the condition under which the insulating material undergoes a sudden change from a low conducting state to a high conducting state under high electric field stress.

A study of dielectric breakdown using a very thin metal electrode to provide "non-shorting" conditions was first reported in 1936.[1] This "non-shorting" technique was then applied to investigate the breakdown properties of thin oxide films in MOS structures by N. Klein et. al. in 1966,[2,3] and was called the "self-healing" technique. In the present study, this "non-shorting" but locally destructive breakdown is referred to as "self-quenched" breakdown (SQBD).

The technique simply utilizes a very thin metal field plate, usually of thickness 1000Å or less, in an MOS structure. The localized breakdown of the oxide provides a conducting filament through which the capacitor-like structure can begin to discharge its stored energy. The tremendous local power dissipation will heat the breakdown spot locally and destroy the oxide and the metal field plate surrounding the filament, thus disconnecting the breakdown spot from the rest of the metal field plate. The insulation of the remainder of the structure is preserved and the sample can be used again.

A simple equivalent circuit of SQBD in MOS structures is shown in Fig. 1-1. The equivalent circuit of the MOS capacitor is enclosed in the dashed line.

C is the total capacitance of the MOS structure,

R_o is the (nonlinear) resistance representing the pre-breakdown conduction,

R_b is the (nonlinear) resistance associated with the conducting filament,

R_L is the load resistance in series with the voltage source V_a.

Closing the switch S simulates the onset of SQBD. Fuse F represents the portion of the thin metal field plate surrounding the filament. The self-quenched breakdown process is schematically depicted in the

semi-logarithmic I-V curve shown in Fig. 1-2, in which I-V characteristics of the nonlinear R_o and R_b are represented by the solid lines I, II respectively. The load line representing R_L in series with V_a is curved on this plane (as is shown by the broken line) because of the vertical logarithmic scale. The load line intersects with curves I, II at the two points A and B respectively. When the applied voltage V_a is increased, the operating point A approaches the switching voltage, whereupon breakdown occurs. If there were no capacitance in the circuit, the operating point would simply shift from A to B instantaneously. The sample might or might not be destoryed, depending on the value of load resistance. Capacitance is present, however, and will keep the voltage from collapsing instantaneously; thus, the operating point moves to point C at the instant of breakdown. The operating point then slides down along branch II (as caused by R_b in the equivalent circuit) toward B. The discharge current of the capacitor, i_c, and the current i_L supplied by the applied voltage source, can be written as

$$i_C = C \frac{dv(t)}{dt} \tag{1-1}$$

$$i_L = \frac{V_b - v(t)}{R_L} \tag{1-2}$$

where $v(t)$ is the voltage across the capacitor.

Assuming $R_o >> R_L >> R_o$, then

$$i_c \approx \frac{v(t)}{R_L} >> i_L$$

for most of the time. (The logarithms of the currents i_c and i_L are shown by dimension lines in Fig. 1-2. Because of our use of a logarithmic scale, actually $i_c >> i_L$.)

The power input from the discharge of the capacitor into R_b can be expressed as

$$p(t) = iv(t) = i_c v(t) = Cv(t) \frac{dv(t)}{dt} \tag{1-3}$$

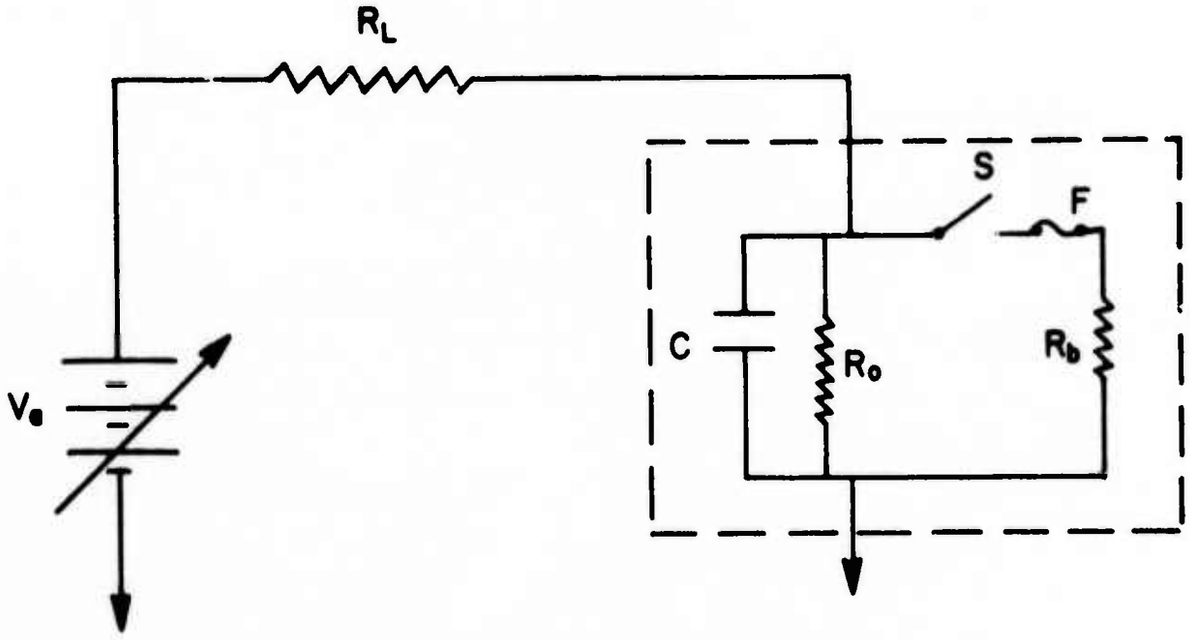

Fig. 1-1 Equivalent circuit of self-quenched breakdown (SQBD) in MOS structures.

If switch S is closed at $t = 0$ when $v(t \leq 0) = V_b$, and assuming for simplicity that R_b has a constant value,

$$v(t) \simeq V_b \exp(-t/R_b C) \tag{1-4}$$

and

$$p \simeq \frac{V_b^2}{R_b} \exp(-2t/R_b C) \tag{1-5}$$

The toal energy dissipation up to time t is

$$U = \int_o^t p \, dt \simeq \frac{1}{2} C V_b^2 [1 - \exp(-t/R_b C)] \tag{1-6}$$

The degree of damage around the conducting filament is determined basically by the joule heating as expressed by Eq. (1-6).

For an MOS sample of oxide thickness d_o, gate area A, and with breakdown field $\mathcal{E}_b$,

$$p = (d_o^2 \mathcal{E}_b^2 / R_b) \exp(-2\kappa\varepsilon_o d_o t / R_b A) \tag{1-5a}$$

and

$$U = \frac{1}{2} (d_o A \mathcal{E}_b^2 / \kappa\varepsilon_o) [1 - \exp(-\kappa\varepsilon_o d_o t / R_b A)] \tag{1-6a}$$

where κ is the dielectric constant of the oxide and ε_o is the permittivity of free space. Thus, an MOS capacitor with a thicker oxide will discharge faster and will have more stored energy to discharge on the breakdown; consequently, the damage caused by the breakdown will be greater.

In general, the damage around the local breakdown filament can be divided into two areas as shown in Fig. 1-3: (1) A large area where the metal gate disappears due to evaporation, melting or other process; this area can be of few microns to few hundred microns in diameter. (2) An inner hole in the oxide, presumably extending through the oxide to the substrate; the diameter of this hole varies from a fraction of a micron to few microns.

Usually the spatial and temporal distributions of these

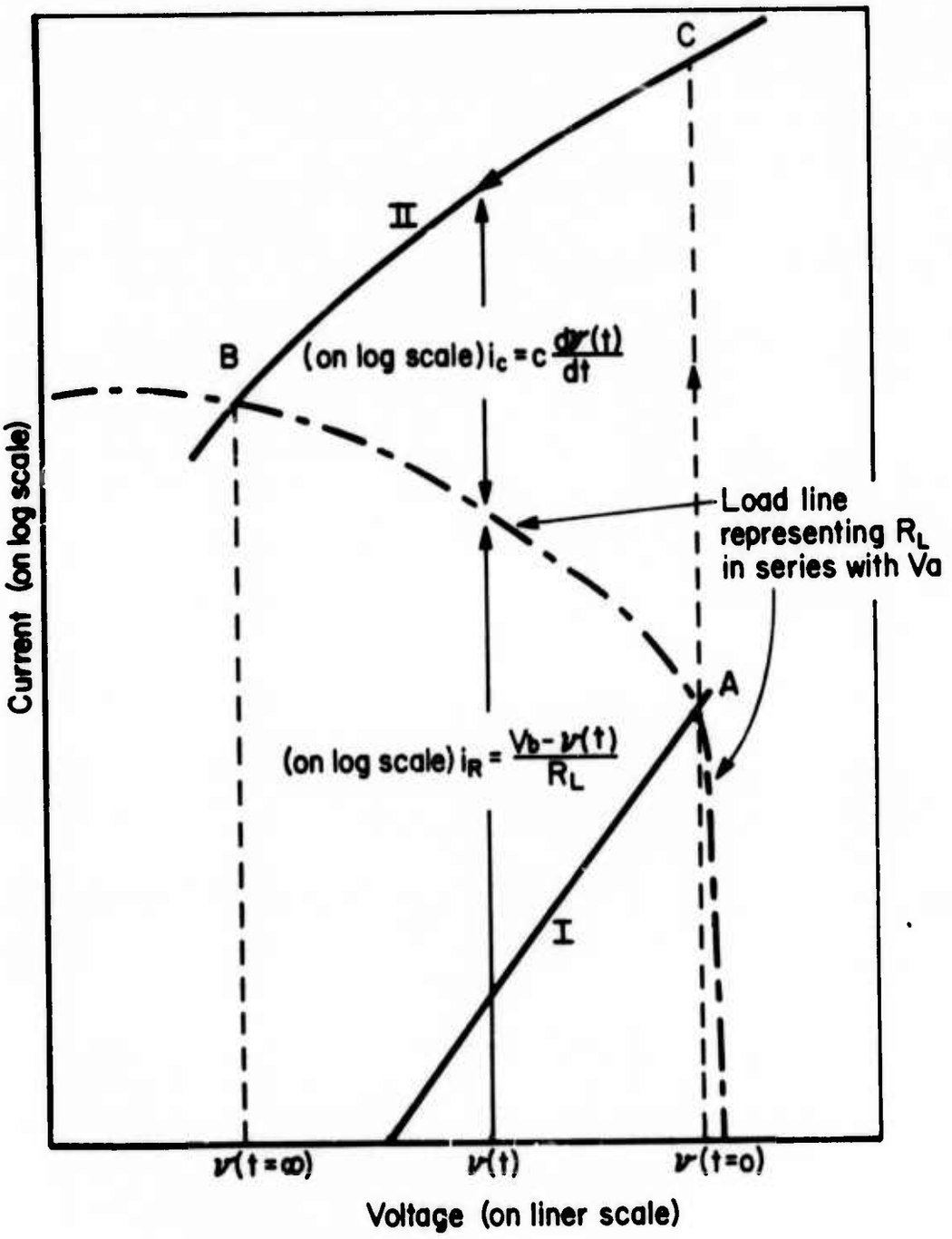

Fig. 1-2 Schematic I-V characteristics for switching process causing breakdown in the MOS structure. Branch I is the I-V characteristic of R_o. Branch II is the I-V characteristic of $R_b << R_o$, Branch II is essentially the I-V characteristic of R_b alone.

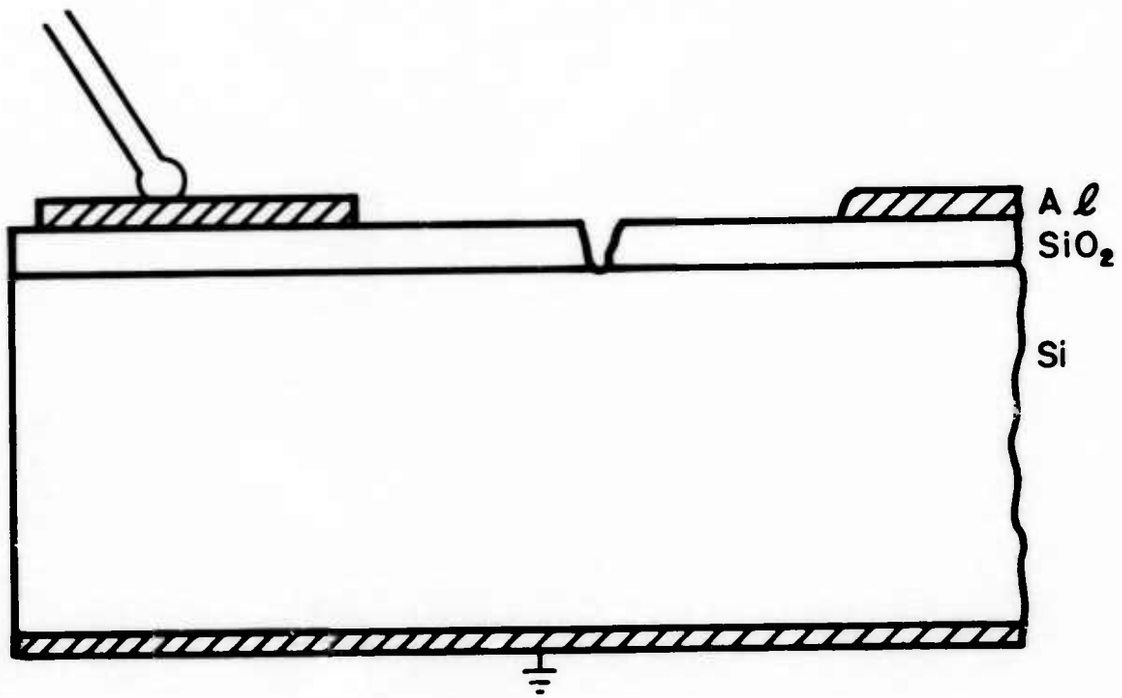

Fig. 1-3 Cross section of a SQBD in a Al-SiO_2-Si structure. (not to scale)

SQBDs are quite random, and the SQBDs happen over a wide range of electric field intensities. The average breakdown rate per unit time increases as the electric field increases.

The main reason for using the self-quenched breakdown technique is simply that with this method a capacitor can be broken down many times until eventually a large portion of it has been damaged. Without SQBD, a sample could be broken down only once, after which it would be shorted permanently; the only data that could be obtained from such a sample would be the lowest breakdown field as caused by the worst defect or weakest spot. Even if numerous data could be obtained by using a large number of samples, the resulting data would represent only a distribution of the strengths of the weakest spots over many samples. The SQBD technique provides a breakdown field profile on a single sample and gives an indication of the "intrinsic" breakdown strength of the insulator by first eliminating the weakest spots without catastrophic destruction of the sample. Since the development of MOS devices, the quality of the thermally grown SiO_2, especially of the oxide under the metal gate, has been a determining factor of yield and reliability. Because of the technological importance of SiO_2 films, the breakdown properties of SiO_2 in MOS structures have been extensively studied. Many of these investigations will be reviewed in Chapter II. Conclusive evidence still remains to be found, however, to account for the initiation of breakdown of thermally grown SiO_2 films in metal-SiO_2-Si structures. The damage mechanism has yet to be clearly understood.

In this study, the experimental investigation emphasizes two areas: (1) The self-quenched breakdown itself -- the study of topographical structure with respect to polarity, substrate type and crystallographic orientation of substrate. (2) The study of high-field conduction and the instabilities which initiate the breakdown. The organization of this thesis is as follows:

Previous investigations are reviewed in Chapter II. Our experimental set-up and samples are described briefly in Chapter III. Chapter IV consists of many micrographs which show the details of the

topographical structures of SQBD in different configurations, together with other observations. Chapter V concentrates on the interpretation of anisotropic SQBD, first observed in this study, and demonstrates further anisotropic SQBDs. Chapter VI consists of a series of electrical measurements in the pre-breakdown region. A model of breakdown initiation is developed from these measured results. The conclusion is given in Chapter VII.

CHAPTER II

REVIEW

The literature on the dielectric breakdown of thin insulating films is reviewed in this chapter. Emphasis is placed on the experimental work done on thermally grown SiO_2 or on other relevant subjects.

General discussions of dielectric breakdown of solids can be found in the following books and review articles:

Dielectric Breakdown of Solids by S. Whitehead.[4]
The Theory of Dielectric Breakdown of Solids by J.J. O'Dwyer.[5]
Electrical Breakdown in Solids by N. Klein.[6]
Dielectric Properties of Thin Films by P.J. Harrop and D.S. Cambell.[7]

Much of the early work on the breakdown of oxide films in MOS structures was done by N. Klein and his coworkers.[2,3,8]

On deposited silicon oxide, Klein[2] observed two kinds of "self-quenched" breakdown. When the series resistance was larger than 10KΩ, he found single-hole breakdown, and when the series resistance was smaller than 10KΩ he found breakdown which propagated from the initial breakdown point and which caused considerable damage. Klein also observed a "maximum voltage" breakdown, which destroyed the whole capacitor simultaneously, after elimination of the weak spots in the oxide by single-hole breakdown. He interpreted this as the result of a thermal runaway process in which the conductivity of silicon oxide is a function of electric field strength and temperature:

$$\sigma = \sigma_o \exp[a\,(T - T_o)] \exp(b\mathcal{E})$$

σ_o is only a fictitious "zero-field" conductivity at $T = T_o$; a and b are two positive parameters. When the silicon oxide was subjected to a high field, the sample was heated up by the joule

heat and the equilibrium temperature was obtained simply by equating the joule heat to the heat lost by heat transfer:

$$\sigma(A/d_o)V^2 = \Gamma (T - T_o)$$

for example,

$$\sigma_o \exp[a(T - T_o)] \exp(b\mathcal{E}) (A/d_o)V^2 = \Gamma (T - T_o)$$

Here, Γ is the thermal conductance of the capacitor unit, A is the area of the electrode, and d_o is the thickness of the oxide.

The maximum voltage could be obtained by a graphical method in which the joule heat input and the heat loss by thermal conductance were plotted as functions of T with voltage as the parameter. The maximum voltage occurred when the joule heat input curve was tangent to the heat-loss line. By manipulating the parameters a and b, Klein obtained good agreement between calculation and experimental results for the value of the maximum dielectric strength.

For single-hole self-quenched breakdown, he argued that the same thermal-runaway process occurred at the local flaws of the oxide.

He also observed self-quenched breakdown, both single-hole and propagating, in MOS structures with thermally grown SiO_2 on (111) silicon substrates.[3] Breakdown was still believed to start with an electric-field-induced thermal instability at a flaw in the SiO_2 which caused a hole to be evaporated through the metal and oxide. In continuation, the capacitor discharged in an arc through the hole, resulting in a relatively large destruction of the metal. The magnitude of the destruction was studied for different polarities and types of substrate. Using oscilloscope traces of the breakdown discharge, he was able to determine the values of the filament resistances and found a dependence on the substrate resistivity.

Budenstein and Hayes[9] studied breakdown conduction in Al-SiO-Al capacitors and proposed a different view for breakdown in deposited silicon oxide. In their model, breakdown was initiated at

a flaw in the SiO. An electron avalanche began at the localized spot in the dielectric. Electrons were injected and increased the conductivity between this breakdown region and the positive electrode. Thus, a high field region formed near the negative electrode, and then the high field caused field emission of oxygen atoms in this region via the electrochemical reaction

$$Si\text{-}O\text{-}Si + (\text{high field}) \rightarrow Si + Si^{+} + O + e^{-}$$

The free oxygen provided the explosive force to remove the electrode metal over the breakdown area. They identified a small bead of polycrystallized silicon in the region of the filament, using transmission electron microscopy. They also found that the critical field decreased with the oxide thickness and was independent of temperature. Contrary to Klein's model, they concluded that the breakdown was not a thermal runaway process because the transition to breakdown occurred very rapidly without a current precursor.

Worthing[10] experimentally investigated the dielectric breakdown of thermally grown SiO_2 with a gold field plate, and noted that the breakdown was polarity-dependent: When the gold field plate was positively biased, the breakdown was time-dependent, following Peek's law. (This refers to the time from the application of constant voltage to the occurrence of breakdown, and depends on the magnitude of the voltage.) This breakdown was attributed to electrical conductance and thermal instability. When the field plate was biased negatively, the breakdown was found to be "time-independent" and to be "intrinsic".

Lenzlinger and Snow[11] studied the high-field conduction in thermally grown SiO_2 of thickness 500Å and 1000Å and reported Fowler-Nordheim tunneling current. Their results were consistent with theoretical calculations except for differences in the effective masses calculated from temperature plots. No breakdown was mentioned although the field intensities used in their study extended to 10^7 V/cm. They also found the current to be proportional to gate area, indicating

that local current filaments did not dominate.

Wang, Van Buren, and Edraos[12] used the scanning electron microscope (SEM) to observe breakdown of thermally grown SiO_2 in the secondary and induced-current modes. They reported that the electron beam enhanced the breakdown of SiO_2 under thin spots in the top aluminum electrode. They argued that electrons were able to penetrate through thin electrodes into SiO_2 and induced breakdown.

Chou and Eldridge[13] studied the effects of material processing and sample preparation on the dielectric strength of thermally grown SiO_2 films in MOS structures. They found that breakdown were insensitive to temperature in the 25-150°C range and that the breakdown field for Al-SiO_2-Si showed no significant dependence on the duration of the applied field -- contrary to Worthing's time-dependent result.

The breakdown of ultra-clean oxide showed few defect-related breakdowns. On regular oxide, the defect-related breakdowns were found to increase appreciably with decreasing oxide thickness. They argued that this was associated with the recrystallization of SiO_2 in amorphous SiO_2, especially after post-metallization heat treatment (e.g., 5 min. at 500°C). Lattice defects created by ion implantation had no effect on the breakdown prior to annealing. Sodium contamination could result in severe oxide deterioration.

Osburn and Ormand[14] found the breakdown strength of thermally grown SiO_2 varied as (oxide thickness)$^{-0.21}$ for oxide thicknesses below 800Å and was constant for oxide thicknesses from 10,000Å to 2000Å. They observed current instability at high field intensities and determined it to be caused by an electronic process rather than a thermal process. The breakdown voltage was the same for oxides grown in wet or dry oxygen, and the oxide growth temperature did not affect the breakdown.

Osburn and Weitzman[15] confirmed the conduction through SiO_2 via the Fowler-Nordheim tunneling mechanism. They also observed current instabilities which were interpreted as being caused by the generation and redistribution of carriers by collision ionization of defect states in oxide. No other evidence was given to support

this model.

Shatzkes, Av-Ron and Anderson[16] proposed the existence of two-branched current-voltage characteristics. Impact ionization was proposed to account for the origin of the switching characteristics.

In summary: The results from those previous studies present an inconsistent picture of dielectric breakdown of thin oxide films, especially of thin SiO_2 films -- how breakdown is initiated and how the damage is caused by the breakdown.

CHAPTER III

EXPERIMENTAL SET-UP AND SAMPLE DESCRIPTION

Our experimental set-up was very simple: the sample was biased by a DC power supply in series with a current-limting resistor, the typical value of which was 1 MΩ. The voltage across the sample was monitored by a Tektronix 585 oscilloscope with plug-in unit A-1 when the breakdown discharge was being studied, or by a digital voltmeter of input impedance of 10 MΩ when I-V characteristics were being measured.

Current through the oxide was measured with a Keithley 415 micro-microammeter. The voltage drop in the ammeter was about a millivolt and thus was negligible. In breakdown discharge studies the ammeter was bypassed by direct grounding. C-V measurements were made at 1 MH_z with a Boonton capacitance meter.

Measurements were conducted either in air or in a vacuum chamber in which the sample temperature could be varied up to 300°C or down to 100°K. When measurements were made in air, the sample was put on a brass block and was flushed continuously with dry nitrogen to keep away dust and moisture. An optical microscope could be set up for direct observation of breakdown. The sample was put in a vacuum chamber whenever high or low temperatures were necessary. The vacuum could be pumped down to 10^{-5} torr.

Care was taken to prevent current leakage in I-V measurements and to minimize the stray capacitance (usually about 1 pF compared to 175 pF oxide capacitance) in breakdown discharge studies and C-V measurements.

The samples have approximately 2500Å SiO_2 thermally grown in dry O_2 on (100) silicon wafers of resistivity about 1 - 2 Ω-cm. Both p- and n-type substrates were used.

Aluminum dots approximately 1000Å thick were vacuum deposited on the exposed surface of the SiO_2. The area of these field plates was about 1.26×10^{-2} cm^2. Almost all of the experiments were made on the above-described samples except for a few experiments on

samples with thicker or thinner oxides. These samples, and the results obtained with them, will be described in Chapter V.

The electrical contact with the field plate was made with a probe mounted on a micromanipulator when the measurement was done in air. The most troublesome problem in this study was the shorting breakdown under the probe; the reason may be (1) the probe penetrated into the oxide and caused premature shorting breakdown, or (2) the contact area was so small that current-crowding induced local heating during charging and discharging of the capacitor. This shorting breakdown under the probe can be avoided by using a soft, smooth probe tip that has a large contact area with the metal field plate to prevent the current crowding without damaging the field plate and penetration of the probe into the oxide. Probes made with gold wire and pure aluminum wire worked very well. When the sample was put into the vacuum chamber, micromanipulation was no longer possible; contact was made using a spring-loaded thin copper foil, and the pressure of the probe on the field plate could not be fine-adjusted as it was when the micromanipulator was used. Therefore, more shorting breakdowns under the probe were encountered when using the vacuum chamber. In that case, the sample had to be taken out and the probe relocated.

CHAPTER IV

EXPERIMENTAL STUDY OF SQBD IN Al-SiO_2-Si STRUCTURES

In this chapter we present the results of an experimental study of self-quenched breakdown itself: the discharge characteristics of a localized breakdown, the topographical details of the self-quenched breakdown damage, the magnitude of the breakdown field, and the effects of scratches made on the metal field plates are investigated for both field plate polarities and for both substrate conductivity types.

IV-1 Experiments

(A) Discharge Characteristics of Al-SiO_2-Si Structures

The voltage across the capacitance, v(t), was monitored using a high-speed oscilloscope. Because the breakdown events are not predictable, the oscilloscope was triggered by the collapsing input signal voltage on the breakdown. A built-in delay line (20-60 nsec) permitted the front portion of the input signal to be seen in each sweep. The results on the 4 breakdown configurations (p-substrate, field plate + and -, and n-substrate, field plate + and -) are shown in the oscillograms in Figs. 4-1, 4-2, 4-3, and 4-4 respectively. Two oscillograms for each configuration are given to show the similarities of discharge characteristics among the localized breakdowns. The samples used are those described in Chapter III.

In each oscillogram, when the field plate is positively biased, the zero-volt level is the bottom line of the graticule; when field plate is negatively baised, the zero-volt line is the top horizontal graticule line. The horizontal trace at the front of each sweep indicates the breakdown voltage (which was delayed by the built-in delay line) for that particular breakdown. The cusp immediately following the brief horizontal sweep is the onset of the breakdown discharge. The discharge of the capacitance caused by the breakdown is shown by the collapsing signal after the cusp. The voltage ceases to drop after certain duration of discharge and begins to increase as a result of recharging of the capacitance from the power supply. Actually, in these oscillograms only the near-horizontal sweeps

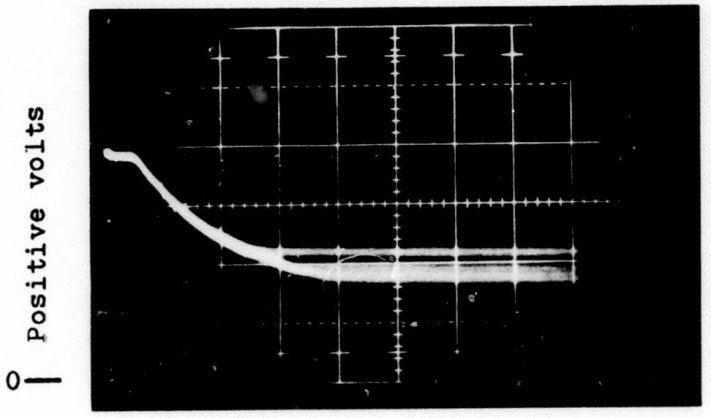

(a) 50V/div., 100nsec/div.; R_L = 1 M Ω

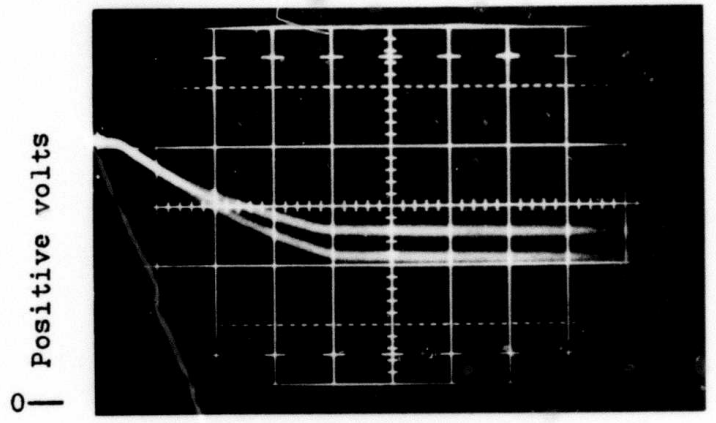

(b) 50V/div., 100nsec/div.; R_L = 1 M Ω

Fig. 4-1 Voltage-time characteristics for localized breakdown of Al-SiO_2-Si structures. d_o = 2500Å, Al(+) on p-type substrates.

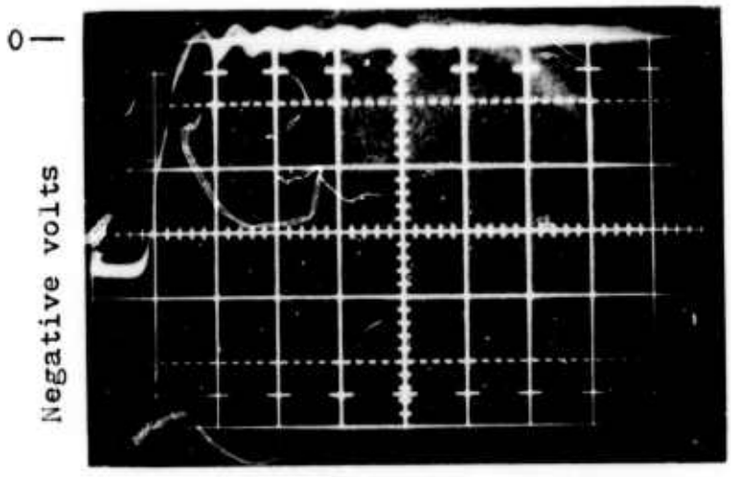

(a) 50V/div., 50nsec/div.; R_L= 1 M Ω

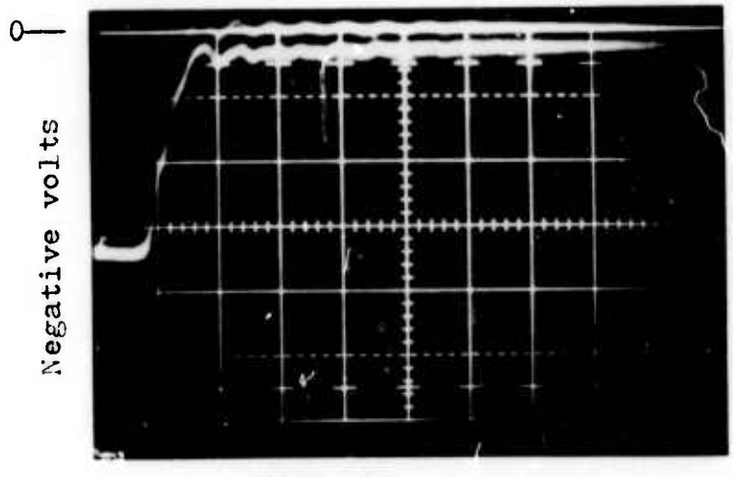

(b) 50V/div., 50nsec/div.; R_L= 1M Ω

Fig. 4-2 Voltage-time characteristics for localized breakdown of Al-SiO_2-Si structures. d_o=2500Å, Al(-) on p-type substrates.

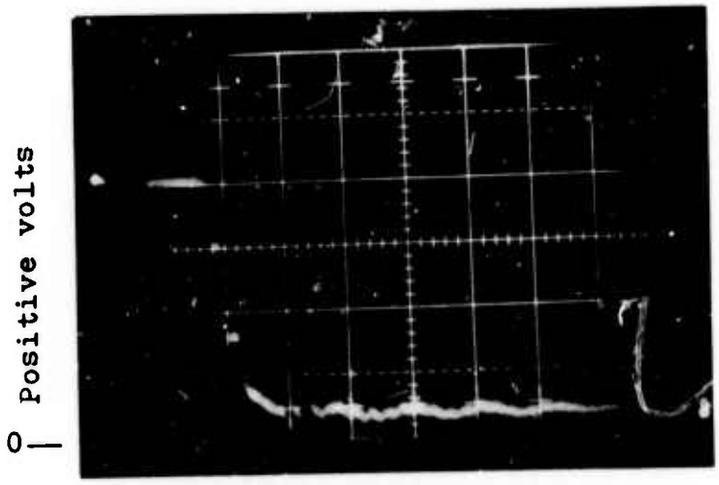

(a) 50V/div., 50nsec/div.; R_L= 1 M Ω

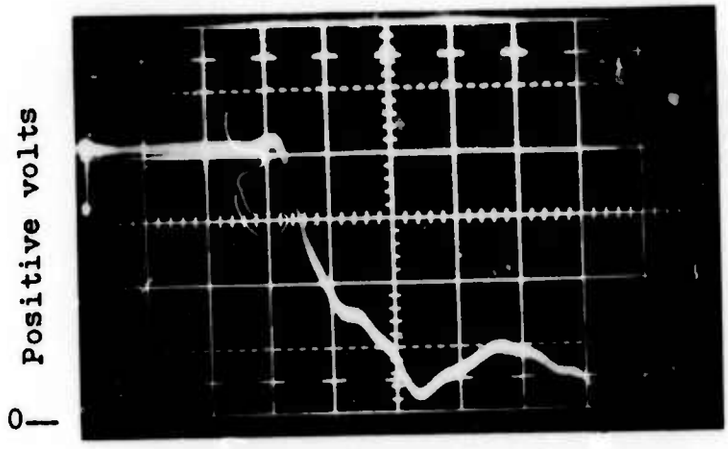

(b) 50V/div., 10nsec/div.; R_L= 1 M Ω

Fig. 4-3 Voltage-time characteristics for localized breakdown of Al-SiO_2-Si structures. d_o= 2500Å, Al(+) on n-type substrates.

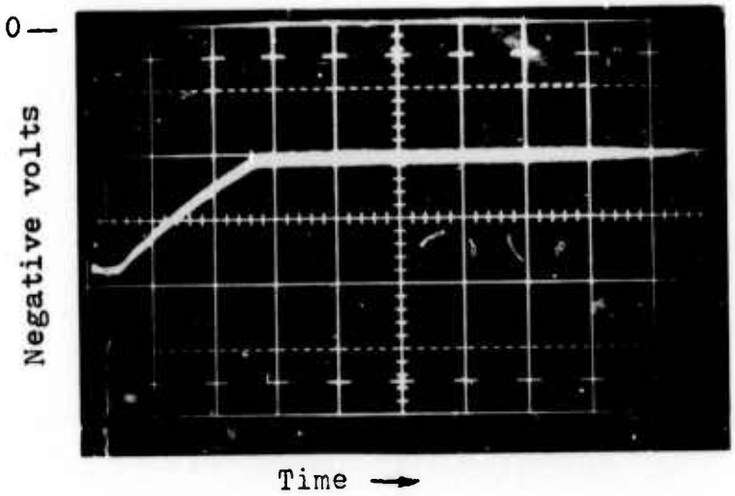

(a) 50V/div., 100nsec/div.; R_L= 1 MΩ

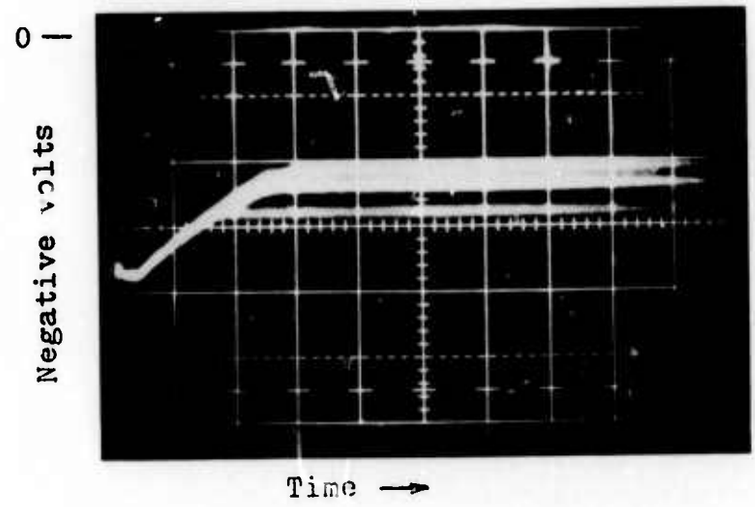

(b) 50V/div., 100nsec/div.; R_L= 1 MΩ

Fig. 4-4 Voltage-time characteristics for localized breakdown of Al-SiO_2-Si structures. d_o=2500Å, Al(-) on n-type substrates.

are seen because of the long recharging time constant (10^{-4} sec. in each case). The turn-around point, at which the voltage stops decreasing and begins to increase, is presumably the instant of self-quenching; i.e., the instant when the damage disconnects the breakdown point from the remainder of the capacitor. In each oscillogram, a couple of traces are shown to indicate the reproducibility of these traces.

The voltage-time oscillograms of these four breakdown configurations apparently can be divided into two distinct groups: (1) Positive-field-plate breakdown on p-substrates in Fig. 4-1 and negative-field-plate breakdown on n-substrates in Fig. 4-4, both of which have long discharge times, about several hundreds of nanoseconds. The minimum voltage after discharge is approximately half of the breakdown voltage. (2) Negative-field-plate breakdown on p-substrates in Fig. 4-2 and positive-field-plate breakdown on n-substrates in Fig. 4-3, both of which have short discharge times of about 20 ns. The voltage drops almost to zero in a short time.

Obviously, the discharge time depends on the conditions in the substrate: in type (1) the substrates are in inversion and the discharge is slow and not complete; in type (2) the substrates are in accumulation and the discharge is fast and almost complete.

Although the voltage-time characteristics are not exact exponentials, an approximate value of equivalent resistance of the discharge path (R_b in Fig. 1-1) can be obtained from the initial slope of the discharge voltage divided by the oxide capacitance as expressed by

$$R_b \simeq v(t = 0)/C(\frac{dv}{dt})_{t=0}$$

The results taken from the oscillograms are:

$R_b \sim 3K\Omega$ when the substrate is in inversion,

$R_b \sim 100\Omega$ when the substrate is in accumulation.

The results suggest that the resistance, R_b, of the discharge path comes from the spreading resistance in the substrate. Some portion of the value of R_b will be contributed by the resistance of filament in the oxide, but the experiment done by Klein[3] showing the dependence of R_b on substrate resistivity indicates that this contribution is small. A further inference to be drawn from this result is that the oxide is almost shorted by the breakdown current filament. The joule heat must be generated in the silicon substrate and the damage must originate from the heat accumulated in the substrate.

(B) The Topography of the SQBD's in Al-SiO_2-Si Structures

After the SQBD's were studied with oscilloscopes, the same samples were put under the optical microscope and in the scanning electron microscope (SEM) for further study. The physical appearance of SQBD's turns out to be distinctly different for each configuration. Optical micrographs are shown in Figs. 4-5 and more detailed SEM micrographs are shown in Figs. 4-6, 4-7, 4-8, and 4-9.

In Fig. 4-5(a) are shown the localized breakdowns on a sample of p-type substrate with both positive and negative field-plate voltage polarities at liquid nitrogen temperature. The near-round breakdown region with ragged edge is a SQBD with negative field-plate polarity. The "square" breakdown regions are the SQBD's with positive field plate polarity. With positive polarity the outer rims are smooth, very different from the ragged edge obtained with a negative polarity. Note that all the corresponding edges of the square SQBD's are parallel to each other and to the 100 crystal axis (indicated in the picture, identified by the cleaved edges of the (100) substrate wafer). The square SQBD's are easily seen when the breakdown occurs at low temperature as liquid nitrogen temperature. When breakdown occurs at room temperature, the SQBD's look rounded as shown in Fig. 4-5(b). The SQBD with negative field plate voltage does not change with the temperature.

Figure 4-5(c) shows an optical micrograph of SQBD's on

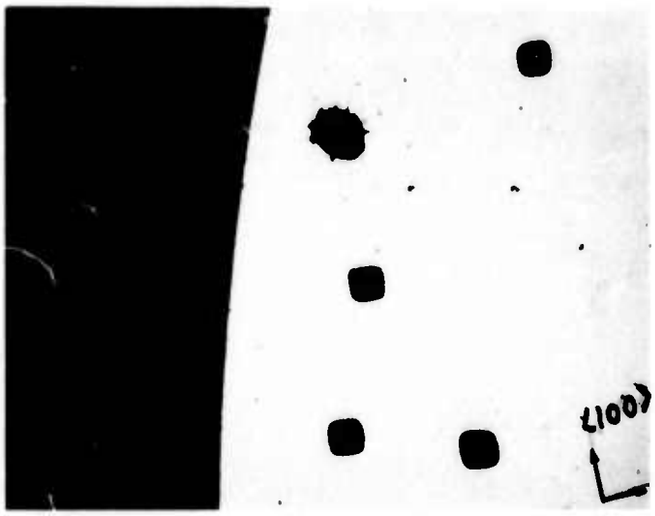

Fig. 4-5(a)

Optical micrograph of SQBD's on (100) p-type substrate with Al(-) and Al(+).
d_o= 2500Å
$V_b \sim 190V$
T= 100°K
X480

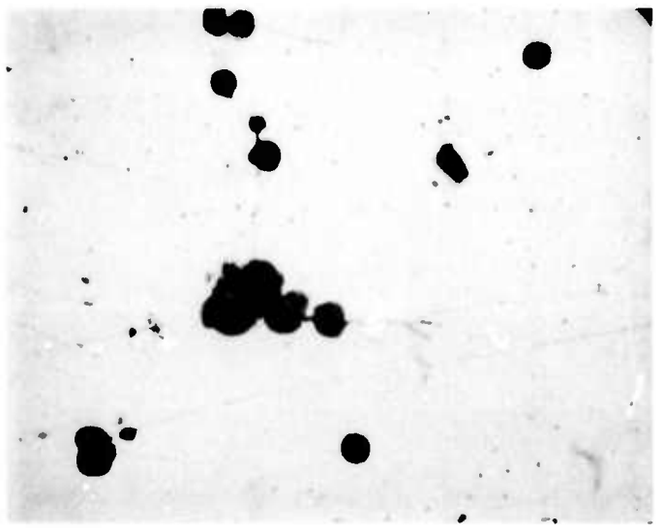

Fig. 4-5(b)

Optical micrograph of SQBD's on (100) p-type substrate with Al(+).
d_o= 2500Å
$V_b \sim 190V$
T= 100°K
X480

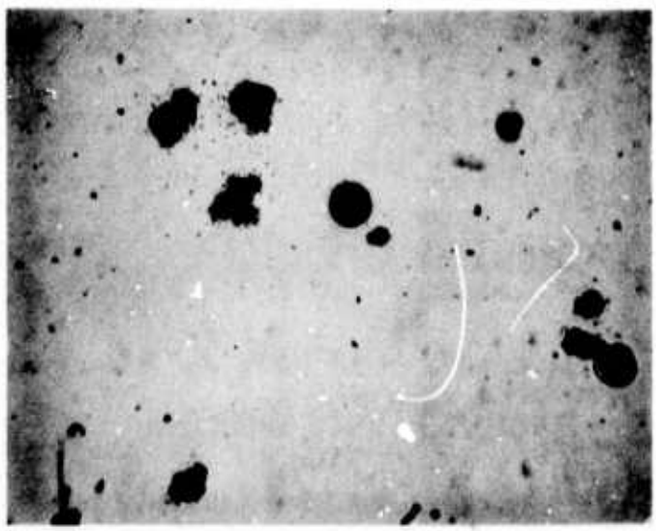

Fig. 4-5(c)

Optical micrograph of SQBD's on (100) n-type substrate with Al(-) and Al(+)
d_o= 2500Å
$V_b \sim 185V$
T= 100°K
x480

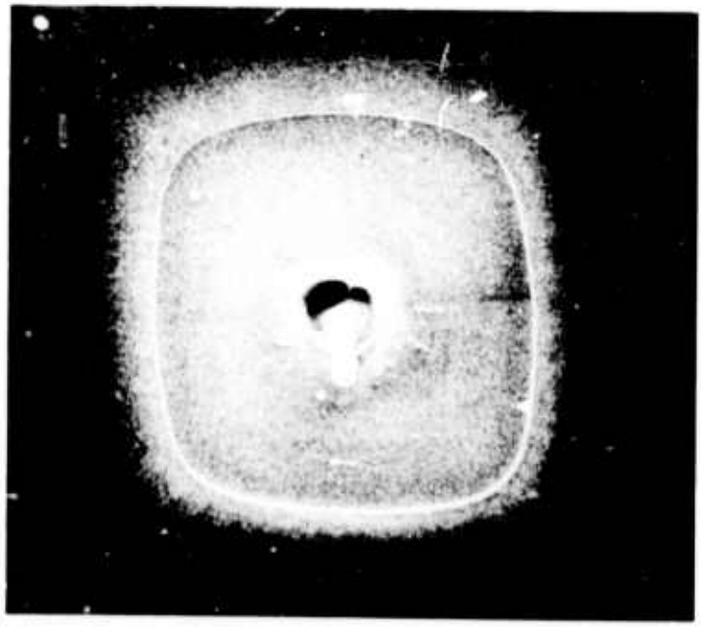

Fig. 4-6 SEM micrograph of SQBD on (100) p-type substrate with Al(+).
d_o= 2500Å, V_b~190V, T=100°K
X5,000

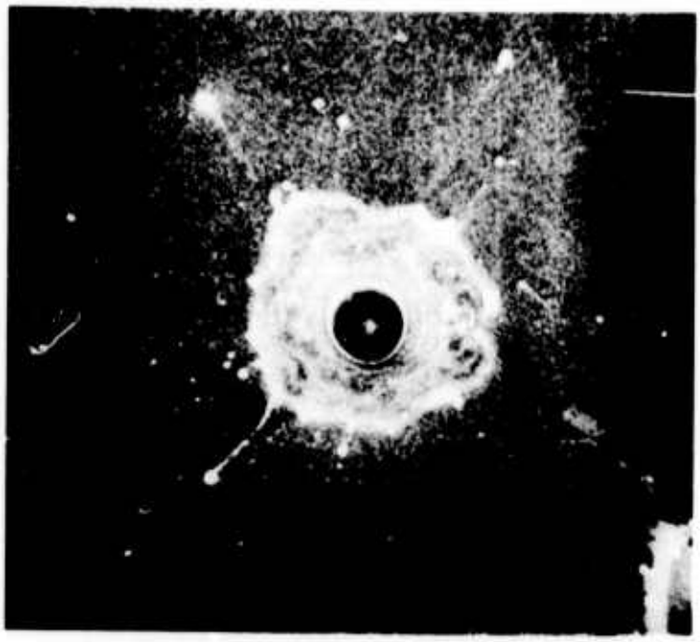

Fig. 4-7 SEM micrograph of SQBD on (100) p-type substrate with Al(-).
d_o=2500Å, V_b~185V, T=100°K
X2,000

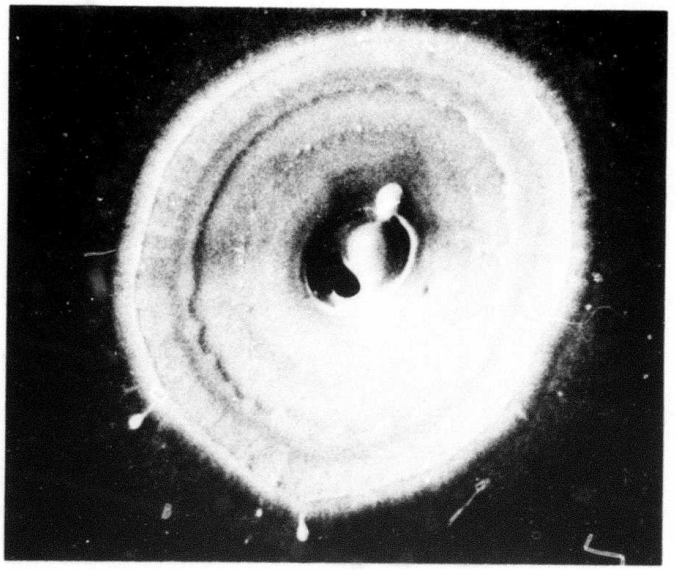

Fig. 4-8(a) SEM micrograph of SQBD on (100) n-type substrate with Al(+).
d_o= 2500Å, V_b~195V, T= 300°K
X5,000

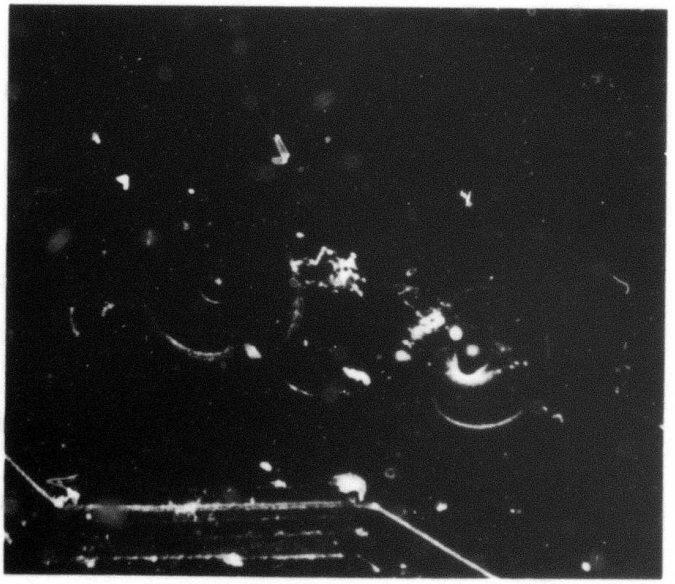

Fig. 4-8(b) SEM micrograph of SQBD nucleated on scratch on (100) n-type substrate with Al(+).
d_o= 2500Å, V_b~180V, T= 100°K
X2,000

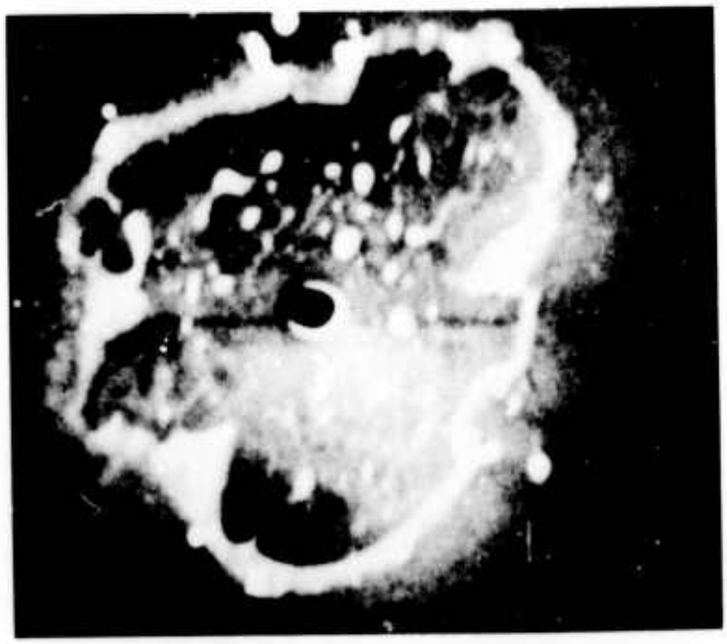

Fig. 4-9(a) SEM micrograph of single SQBD on (100) n-type substrate with Al(-). d_o=2500Å. V_b~185V, T= 300 °K
x5,000

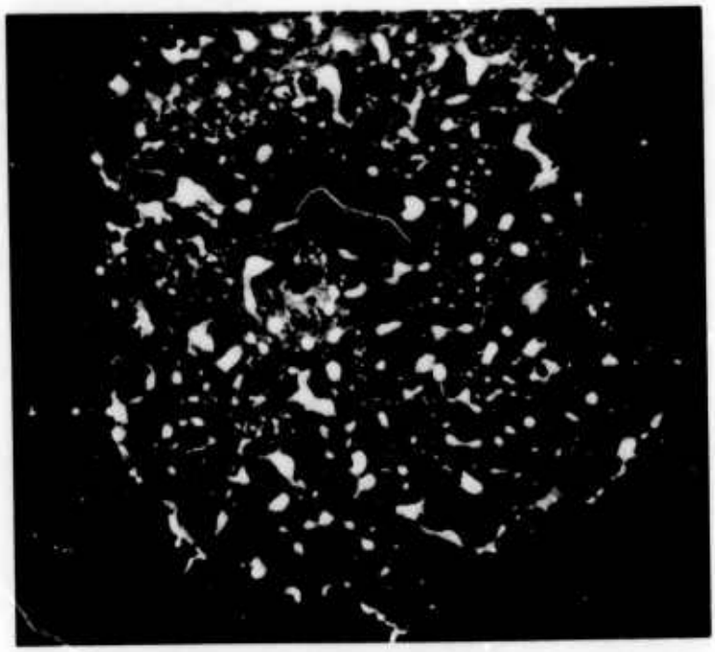

Fig. 4-9(b) SEM micrograph of "multiple" SQBD on (100) n-type substrate with Al(-). d_o=2500Å, V_b~185 V, T= 100 °K
x2,000

n-type substrate with both polarities. The round and smooth-rimmed SQBD's are positive-field-plate breakdowns. The irregular ones with ragged edges are negative-field-plate breakdowns. Note the numerous dust-like tiny black dots around the negative SQBD's. These SQBD's do not show any crystallographic orientation dependence or temperature dependence.

In Fig. 4-6 is shown the SEM picture of positive-field-plate breakdown on p-type substrate. The outer dimension of the square is about 10 μ and the diameter of the inner hole in the oxide is about 2 μ. The outer rim is very smooth and clear, just as was seen in Fig. 4-5(a). Some molten material seems to have split over from the inner hole.

In Fig. 4-7 an SEM micrograph of SQBD on p-type substrate with field plate negative shows the "ragged edge" as "splashed" molten metal that seems to result from a volcano-like explosion. The inner hole is larger than that in Fig. 4-6, about 5μ in diameter. The boundary between the metal field plate and the oxide is not so clear as that shown in Fig. 4-6. The overall size is a little larger than the square one.

Figures 4-8(a) and (b) are SEM pictures of SQBD's on n-type substrate with field plate positive. The features are (1) the smooth and round outer rim and (2) the bigger inner hole (3-5μ in diameter). Figure 4-8(b) shows two SQBD's nucleated on a scratch on the Al field plate.

In Fig. 4-9(a) and (b) are shown SQBD's on n-type substrate with field plate negative. Figure 4-9(a) is a single SQBD. Figure 4-9(b) shows a "multiple" SQBD which is distinct with multiple inner holes (6 in this picture). This "multiple" SQBD, often observed in this breakdown configuration, is believed to consist of many single SQBD's clustering together. The features are (1) the "splashy" edges and the small inner holes (1-2 μ in diameter).

(C) The Effects of Scratches

Scratches, made on the Al field plate either deliberately or unintentionally, are found to affect the breakdown only when the field plate is positive in polarity.

This fact was first observed on two adjacent samples scratched at the same time and in the same manner with a diamond-tipped scribe. When the Al field plate was biased negatively, the SQBD's distributed themselves randomly and did not nucleate particularly on the scratches. But when the field plate of the adjacent sample was biased positively, the SQBD's all nucleated on the scratch at a lower-than-usual voltage. There is no reason to believe that the scratches were different on these two samples. Moreover, other tests were done on other samples of different substrate type and with scratches made deliberately. The choice of these samples to be scratched was quite random. All results tend to confirm that the first observation was quite typical. Scratches only affect SQBD when the field plate is positive in polarity.

This effect is best illustrated in the series of micrographs shown in Fig. 4-10. This sample of n-type substrate was first biased with field plate negative to 185V, and then was biased with the opposite polarity to 180V. The almost overall view at magnification 72 in Fig. 4-10(a) shows SQBD nucleated on 4 faults pointed by arrows and other SQBD's distributed randomly. The lower-left nucleation is magnified in Figs. 4-10(c) and 4-10(d) in which the SQBD's can be identified by their appearance to be Al-negative breakdowns. But there is no scratch there! This fault apparently lies beneath the field plate and is revealed by the Al-negative SQBD's.

Figures 4-10(a), (b) and (e) clearly show that the SQBD's which nucleate on the surface scratches are field-plate-positive SQBD's. The random SQBD's are field-plate-negative SQBD's.

The evidence is very clear that Al field-plate-negative SQBD's tend to ignore the scratches <u>on</u> the Al field plates and Al field-positive SQBD's tend to nucleate on the scratches and at

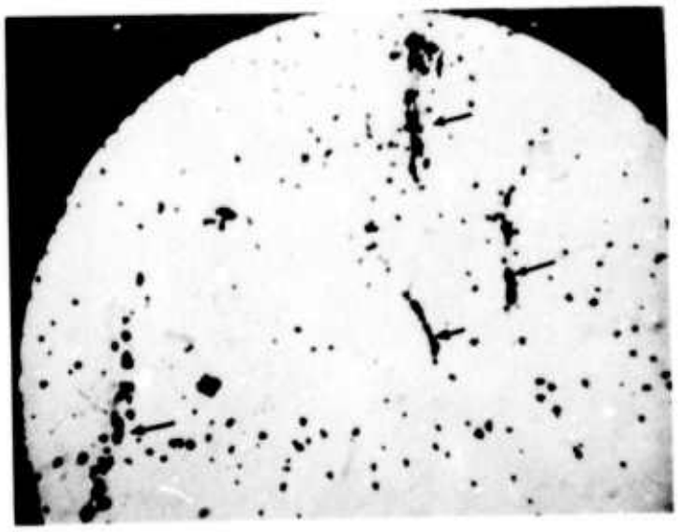

Fig. 4-10(a)

X72

Fig. 4-10(b)

X120

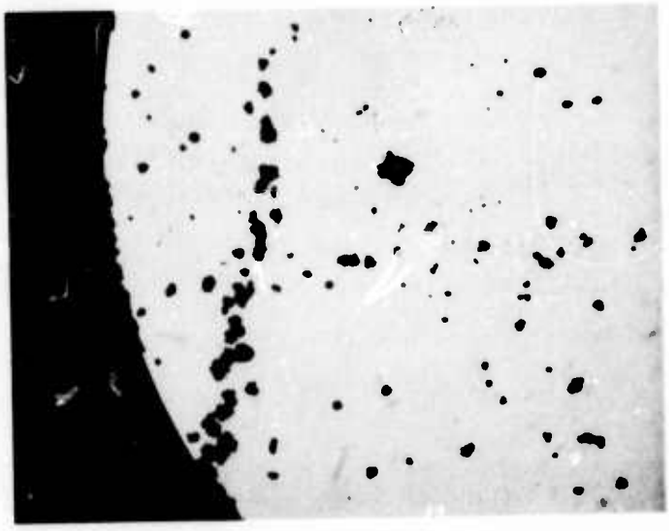

Fig. 4-10(c)

X120

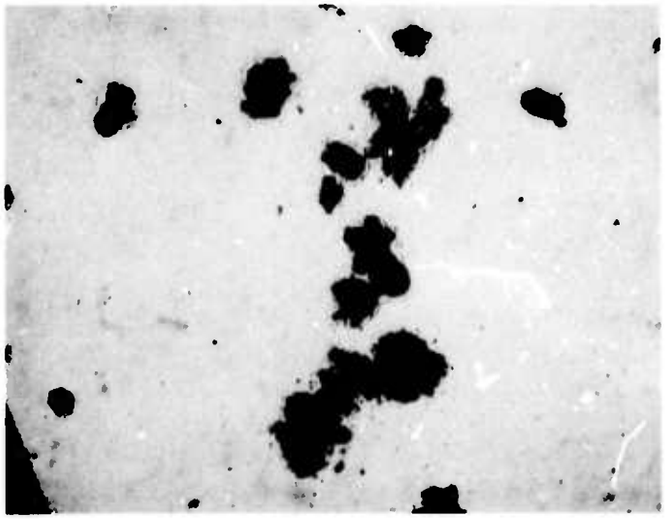

Fig. 4-10(d)

X480

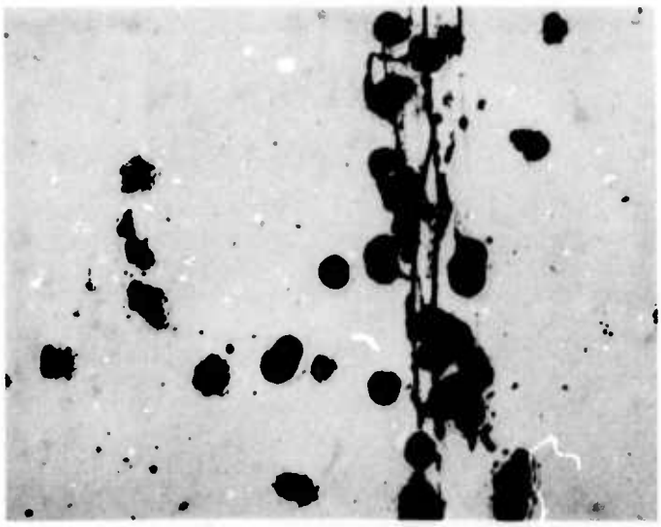

Fig. 4-10(e)

X480
SQBD's with Al(+),
nucleated on scratch.

Fig. 4-10 Optical micrographs showing the distribution of SQBD's on a scratched Al-SiO_2-Si(n-type) structure.
d_o = 2500A, first biased with A(-), V_b = 185V; then biased with Al(+), V_b = 180V.

lower breakdown voltage.

In the foregoing we have, of course, distinguished the SQBD's of the different field-plate polarities by their different topographical appearances, as was described in the preceding section.

(D) The Distribution of Breakdown Voltages

Since only samples of the same thickness were used in this particular portion of our work, the average electric field intensity is directly porportional to the applied voltage.

The breakdown voltage V_b is an ill-defined term. So far, it has been used to indicate the voltage at which a particular breakdown event occurs or the maximum voltage ever applied to the field plate of the samples to produce the SQBD's as in Section C. Since the SQBD's can occur over a wide range of applied voltage, the breakdown voltage can only be defined in a statistical way in studying the average dielectric strength of the oxide film or the average breakdown properties of MOS structures.

The distribution of the breakdown voltage, for example, are shown in Fig. 4-11 in which the abscissae indicate the average value of electric field intensity at which the sample is biased. The electric field is increased by 2×10^5 V/cm each time and then is held for 15 minutes. The number of SQBD's that occurred in this period is plotted as the ordinate. The effects of polarity, temperature, and the scratch on the field plate are shown in Fig. 4-11. The dashed lines with arrows represent continuous breakdown events at a rate of about 1-2 per second.

On the samples used in this study, the Al-positive breakdowns have higher "breakdown" fields ($\sim 8 \times 10^6$ V/cm) than the Al-negative breakdowns ($\sim 7.6 \times 10^6$ V/cm) at room temperature, independent of substrate type. At 100°K, the "breakdown" field seems to shift toward lower field intensities for both polarities. Scratches increase the number of SQBD's at lower field intensities for Al-positive breakdown, but this is not so clearly true for Al-negative breakdown; however, this comparison was made on only two samples and cannot be regarded as conclusive.

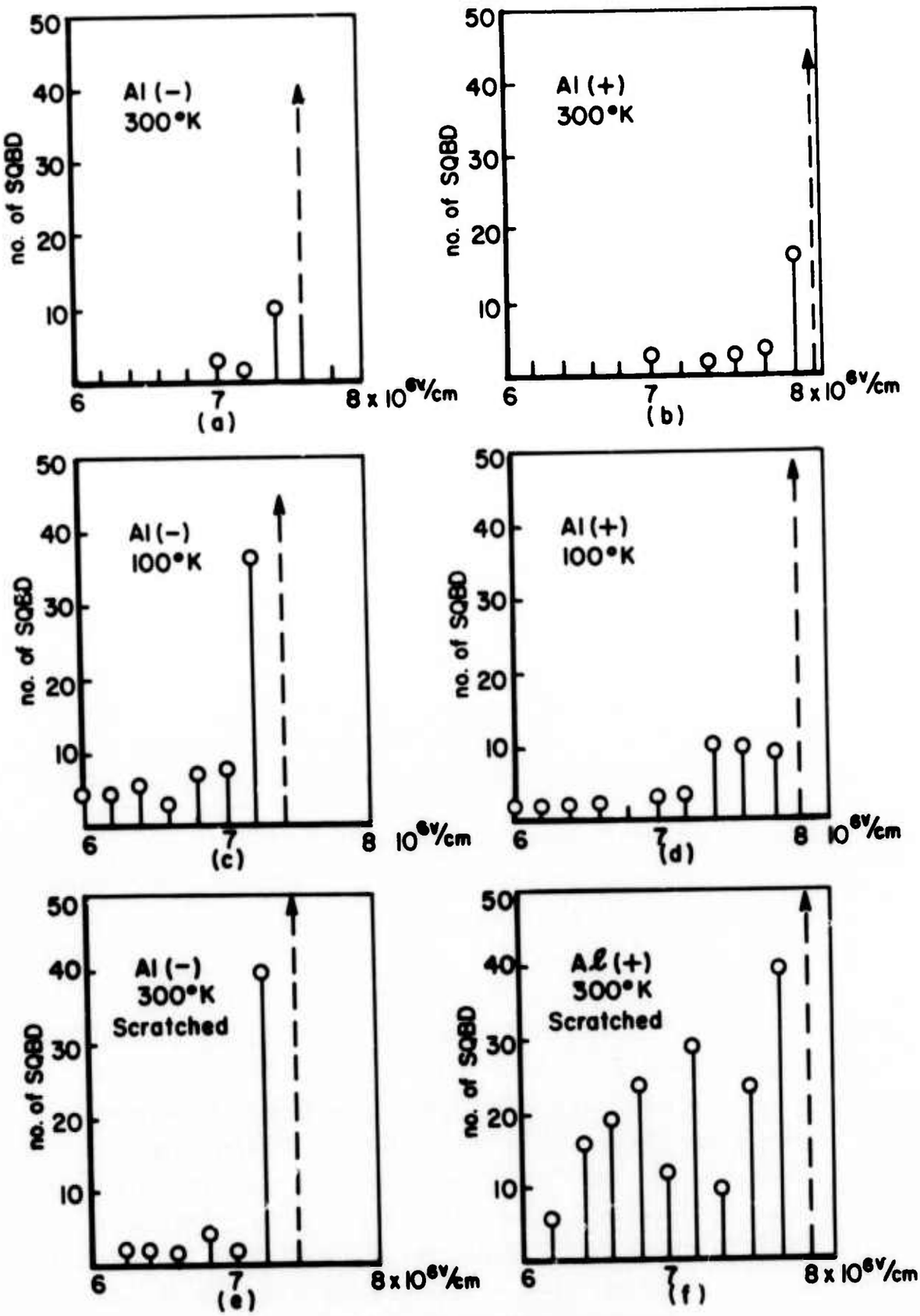

Fig. 4-11 Distributions of breakdown field on Al-SiO_2-Si structures. d_o = 2500Å, (dashed line and arrow representing high breakdown rate: 1∿2 BD/sec)

IV-2 Summary and Discussions

The experimental results are summed up in Table I. Some correlations between the topography of damage, field plate polarity, and substrate type are as follows:

(1) The substrate conditions (inversion or accumulation) are important factors determining the shape of the damage in SQBD's and their discharge characteristics: the accumulation of the substrate provides a fast breakdown discharge path of low resistance and causes a large hole in the oxide. Inversion in the substrate increases the resistance for discharge and results in a small hole in the oxide.

Estimation of the initial current density by assuming the current is confined to a region having the same dimension as the inner hole is as follows:

$$j_b = \frac{C\ dv/dt]\ t = 0}{\text{Area of Inner Hole}}$$

Using this expression we obtain:

For accumulation: $j_b \sim 10^8$ A/cm^2

For inversion: $j_b \sim 10^7$ A/cm^2

The high current density apparently is the major factor in creating damage and is limited by the resistance in the substrate.

(2) The effect of field plate polarity on the shape of SQBD is very obvious: when the field plate polarity is positive, the SQBD's have smooth outer rims; when the field plate is negatively biased, the SQBD's have "splashed" outer rims regardless of substrate type. This difference strongly suggests two different damage processes corresponding to the field plate polarities.

In spite of the results obtained so far, only qualitative correlations can be found since the only quantitative data are the discharge characteristics from which the time-dependent power input can be calculated. The final damage can only give some hints about

Table I: Summary of Self-Quenching Breakdown Properties of Al-SiO_2-Si Structures Fabricated on (100) Oriented Substrates

		Positive Field-plate Polarity	Negative Field-plate Polarity
p-Type Substrate	i)	substrate in inversion	substrate in accumulation
	ii)	discharge time constant: tenths of μsec	discharge time constant: ≈ 10 nanosec
	iii)	smooth outer rim	'splashed' outer tim
	iv)	scratch-nucleated breakdowns	no scratch nucleation
	v)	center-hole diameter: ≈ 2μ	center-hole diameter: ≈ 5μ
	vi)	crystallographic orientation	no crystallographic orientation
n-Type Substrate	i)	substrate in accumulation	substrate in inversion
	ii)	discharge time constant: ≈ 10 nanosec	discharge time constant: tenths of μsec
	iii)	smooth outer rim	'splashed' outer rim
	iv)	scratch-nucleated breakdowns	no scratch nucleation
	v)	center-hole diameter: ≈ 3-5μ	center-hole diameter: ≈ 1-2μ
	vi)	no crystallographic orientation	no crystallographic orientation

what really happened during the breakdown discharge process.

Since the exact spatial distributions of current density J and of electric field are not known during the breakdown, the interpretation of all the different topographical structures relies on guess and speculation.

Fortunately, the field-plate-positive SQBD's on p-type substrates, which show strong dependence on the crystallographical orientation of the (100) substrate, make it seem certain that in this case the origin of the damage of the metal field plate is in the substrate, and the field-plate damage may have the same pattern as the heating pattern in the substrate. This not only explains the crystallographic orientation dependence of the square SQBD's but also explains the smoothness of the outer rim: this may be the result of evaporation and partial melting by the heat conducted from the substrate through the oxide. Then the same argument can be applied to the smoothness of the outer rim of field-plate-positive SQBD on n-type substrate samples, although here there is no crystallographic orientation dependence (see next chapter).

The "splashy" edges of the SQBD when the field plate is negatively biased can be explained in a hypothetical way by assuming that the current which flows through the filament in the oxide consists of electron current only. In other words, the electrons are extracted from the substrate into the oxide when a positive-field-plate breakdown occurs and the electrons are injected into the substrate from the oxide during a negative-field-plate breakdown. The possible different flow patterns under high field in the substrate would certainly result in different spatial distributions of joule heating and temperature which accordingly would cause different damage patterns: with positive-field-plate breakdown, the current is mainly the inversion current in the p-type substrate, and consists partly of the current flow along the more conductive accumulation layer in n-type substrate. The current flow along the SiO_2-Si interface might provide enough joule heat at the interface which would pass through the oxide and melt and evaporate the thin metal field plate locally. This would result in a smooth outer rim

in each SQBD.

With field-plate-negative breakdown, the electrons would be injected into the silicon substrate in high fields and would recombine with holes mostly in the bulk because of the small probability for electrons to recombine in the thin inversion layer or accumulation layer. Since it is assumed that the hole current, the lateral hole current flowing along the SiO_2-Si interface might be very small enough so as not to be able to generate sufficient joule heat. The current density and joule heating might concentrate right underneath the current filament in the oxide and cause evaporation in the Si, thereupon pushing the heated field plate outward like the explosions of a volcano. The tiny particles around a negative-field-plate SQBD, as seen in Fig. 4-5(c), might be the "debris" of the explosion.

Finally, the conclusions can be stated as follows:

(1) The breakdown discharge is controlled by the spreading resistance in the silicon substrate and consequently the joule heat is generated in the silicon substrate and the damage originates from the heating of the silicon substrate.

(2) The SQBD's of 4 configurations can be distintuished by their distinct topographical details which can be correlated to the field plate porarities and substrate conductivity-type. The polarity-dependent topographical structures may result from different current flow patterns in the substrate.

CHAPTER V

ANISOTROPY OF SQBD IN Al-SiO_2-(100) p-Si WITH POSITIVE POTENTIAL ON THE FIELD PLATE

In Fig. 4-5(a) and Fig. 4-6, square SQBD's are exhibited which have substrate crystallographic orientation dependence. To our knowledge, these were the first anisotropic SQBD's ever observed in MOS structures.

The study of anisotropic breakdown is not new, however, previous breakdown studies on alkali-halides had shown that breakdown can have preferential directions in a crystal regardless of the direction of the applied field.[17,18,19] Anisotropic tracking on silicon surfaces was reported by Harman,[20] who observed that tracking was always found along the <100> direction independently of the direction of the forward applied field. However, the anisotropy observed in our study has a different physical nature -- the breakdown occurs in the SiO_2 insulator, not in the semiconductor, and the damage to the metal field plate reflects the crystal orientation of the substrate wafer which, itself, is believed not to be involved in the initiation of the breakdown.

V-1 The Interpretation of Anisotropic SQBD

In Chapter IV, it was concluded that on the occurrence of SiO_2 breakdown, the discharge rate is controlled by the resistance of the substrate, not by the current filament in the oxide and not by the metal field plate. That means that the voltage that existed across the oxide prior to breakdown, and which is maintained temporarily by the capacitance of the undamaged portion of the structure, is impressed mainly on the silicon substrate immediately after the onset of breakdown. When the Al field plate is biased positively on an MOS capacitor with p-type (100) substrate, there exists, prior to breakdown, an equipotential n-type inversion layer. When breakdown occurs, the oxide is temporarily shorted at the point of failure. Then almost the full applied voltage appears laterally in the n-type inversion layer about the point of failure,

resulting in large radial current along the inversion layer into the shorting current filament in the oxide. An anisotropic current pattern is produced by an anisotropy in the conductivity of the 2-dimensional inversion layer on the (100) substrate (discussed in the next section): at high field intensities, the electronic conductivity along <100> directions is smaller than that in the <110> directions in silicon. The result of this is that the current densities along the <110> directions are greater than the current densities along the <100> directions. Accordingly, the joule heat generated at the interface along <110> is higher than that along <100>. Because of the planar geometrical structure, the lateral heat conduction can be neglected. The anisotropic joule-heat pattern is transferred to the metal field plate after the heat conducts through the thin oxide films; thus the metal of the field plate is melted and evaporated according to the anisotropic heating pattern.

This interpretation not only explains satisfactorily the square SQBD observed with p-substrate and positive field-plate polarity but also explains the isotropic SQBD's observed with n-type substrate and positive field-plate bias: in this configuration the substrate is in accumulation, and hence the current flow will not be confined to the (100) face of the substrate but will extend into the bulk; thus the anisotropy of conduction on the (100) face is lost. As is discussed in the next section, the anisotropy of hot electron conduction in silicon (and in germanium) is the result of the many-valleyed character of the conduction bands in these materials. By contrast, the valence bands in these materials are almost symmetrical about $k = 0$ in reciprocal space. This explains the absence of anisotropic damage in SQBD's with n-substrate and field-plate negative in polarity. Also, when the field plate is negatively biased, the damaging process is presumably different, as evidenced by the "splashy" edge.

V-2 The Origin and Properties of the Anisotropy of Hot Electron Conductivity in Many-valleyed Semiconductors

The anisotropy of hot electron conductivity in many-valleyed semiconductors at high fields was first pointed out by Subiyu.[21(a)] The most prominent materials with this characteristic are germanium with eight constant-energy ellipsoids in the <111> directions and silicon with six constant-energy ellipsoids in the <100> directions. The existence of anisotropic conduction in such materials was first confirmed on n-germanium by Sasaki and Subiyu.[21(b)]

A general review of this area can be found in Chapter II of the book High Field Transport in Semiconductors by E. Conwell.[22] We will give here an explanation of high-field anisotropic conduction in multi-valleyed semiconductors based on Sasaki, Shibuya and Mizuguchi[21(c)] and Conwell.[22]

Figure 5-1 is drawn for silicon, where the conduction band minima are along the six equivalent [100] directions. The surfaces of constant energy are ellipsoids, as shown. Consider the contribution to current of two representative groups of electrons which, in thermal equilibrium, occupied states at or near the two conduction band minima located at k_{xo} and k_{yo}, respectively, in Fig. 5-1. An electric field of intensity $\mathcal{E}$ has caused the electrons to be translated in k space by the time average amount $\delta k = -q\bar{\tau}\mathcal{E}/\hbar$ where $\bar{\tau}$ is the mean free time.[23] If the electric field is small, neither set of electrons will be heated up appreciably, the mean free times will be the same for both, and the amount of the translations in k space will be the same for both. The figure shows the electric field applied in a direction more nearly parallel to the long axis of ellipsoid B, and as a result ellipsoid B is smaller than ellipsoid A and the electrons in ellipsoid B at a lower energy and are correspondingly cooler than thos in A. The electron velocities are the wavepacket group velocities given by $\vec{U} = (1/\hbar)\,\mathrm{grad}_k E$ where E is the energy, and their directions are normal to their respective ellipsoids. Each individual contribution to current is proportional to number of electrons times electron velocity, and the

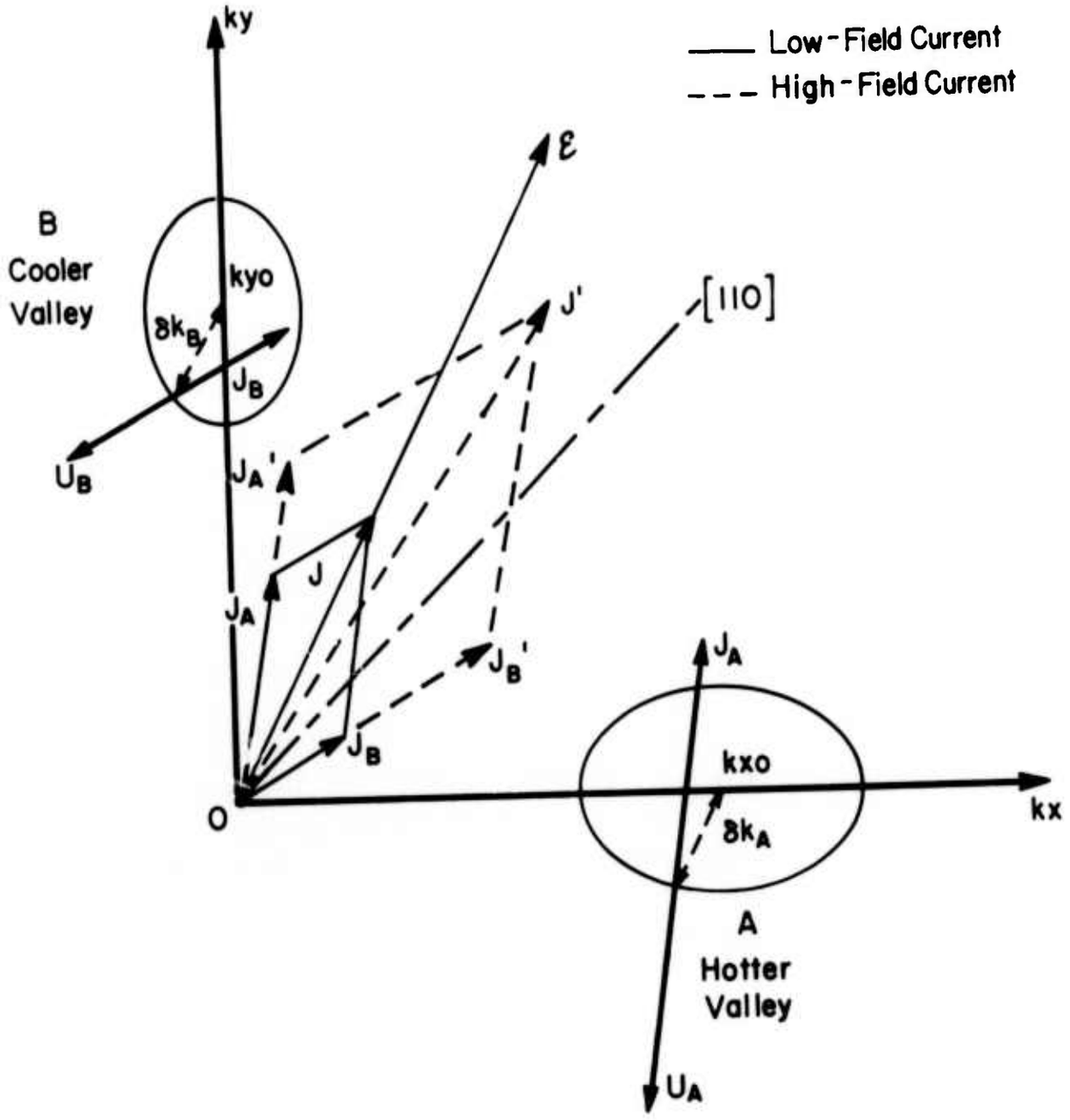

Fig. 5-1 Spheroidal energy surface model for explaining high-field anisotropy.

two contributions are designated as J_A and J_B, respectively, in the figure. The resultant current density, J, lines up with the direction of the electric field.

At high fields, however, two factors change, and both alter the result in the same direction. First, the electrons in valley A, being hotter, have a smaller mean free time than those in valley B; hence k_A is smaller than k_B and the electrons in valley A make less than their proportional contribution to J_A. Second, electrons will be scattered, on the average, from the hot valley into the cold valley, thus increasing the current contributed by the cold valley. The result is shown by the dashed lines In Fig. 5-1, where J_B' is disproportionately large compared with J_A' and the resultant high-field current, J', is inclined away from E toward the [110] axis. The effect is an anisotropy with the conductivity in any of the equivalent [110] directions greater than the conductivity in any of the equivalent [100] directions. As the electric field intensity is increased still more, the electrons in the formerly cool valleys will become heated also, and the anisotropy will diminish. Experimental results for silicon are shown in Fig. 5-2.

In general, the properties of this anisotropy can be summed up as follows from theoretical considerations and experimental results:

(1) At low temperatures, the anisotropy is more pronounced than that at high temperatures.

(2) The anisotropy decreases as the concentration of carriers increases.

(3) The anisotropy starts to occur at electric fields about several hundred volts/cm and increases as the field increases until it reaches a maximum at a certain field. Then it decreases as the electric field increases further to about 10^5 V/cm. The fields of the onset of the anisotropy and of the maximum anisotropy and of the vanish of the anisotropy depend on the temperature and carrier concentration.

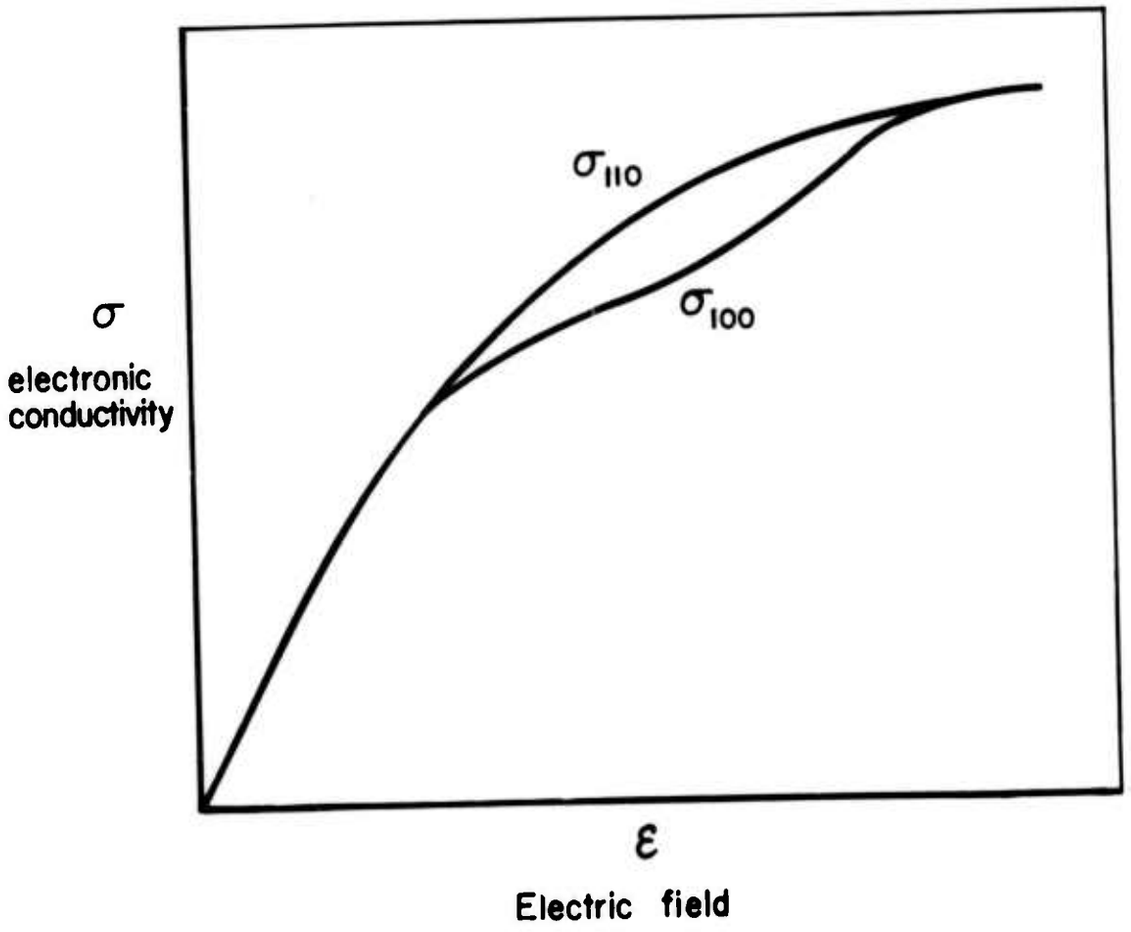

Fig. 5-2 Schematic diagram for hot-electron conductivity. σ_{100} is the conductivity along <100> when field is in <100> direction and σ_{110} is the conductivity when electric field is in <110> direction.

V-3 Schematic Model and Prediction

We have already seen in Figs. 4-5(a) and (b) that a 2500Å oxide shows anisotropic SQBD damage clearly at 100°K but much less clearly at room temperature. As was mentioned in the preceding section, the anisotropy will increase as the electric field increases particularly if the anisotropy is at the onset stage. As the breakdown errupts, almost the full amount of the voltage drops across the silicon. A higher breakdown voltage will give a higher field in the silicon after breakdown; consequently, greater anisotropy.

A simple schematic model is constructed below to explain the possible SQBD pattern with greater anisotropy.

As the breakdown occurs, the current density in the inversion layer can be written as

$$\vec{J} = f(\theta)/\hat{r}$$

The function $f(\theta)$ represents the anisotropy and is a suitable function of angle θ. The local joule heat generated by the lateral current flow in the n-inversion layer is

$$\vec{J} \cdot \vec{\mathcal{E}} \sim J_r \mathcal{E}_r \propto f(\theta)/r^2$$

Here it is assumed that the electric field is isotropic and proportional to 1/r (this functional form would preserve the validity of

$$\vec{J} = (\text{constant})\vec{\mathcal{E}} \quad \text{and} \quad \nabla \cdot \vec{J} = 0)$$

Then the contours of constant joule heat are given by

$$r^2 \propto f(\theta)$$

A simple choice for $f(\theta)$ which has the hot-electron conductivity along <100> and which would produce the anisotropy is

$$f(\theta) = 1 + K(V_b)\sin^4 2\theta$$

$$K(V_b) = (\sigma_{110} - \sigma_{100})/\sigma_{100}$$

$\sigma_{110} \geq \sigma_{100}$ in silicon.

θ is measured from the <100> direction,

σ_{110} the conductivity along <100> direction,

σ_{100} the conductivity along <100> direction,

V_b is the breakdown voltage.

If K = C, i.e., if $\sigma_{110} = \sigma$ [illegible], the breakdown pattern should be round. In general, the [illegible] $_x(\theta = 45°)$ to $r_{min}(\theta = 0°)$ is

$$r_{max}/r_{min} = (k + 1)^{1/2} = (\sigma_{110}/\sigma_{100})^{1/2}$$

The contour $r = \sqrt{f(\theta)}$ are plotted in Fig. 5-3 for K = 0, K = 0.5, K = 3, respectively. It is seen that K = 0.5 is quite squarish as are the breakdown contours in Fig. 4-5(a) and Fig. 4-6. The contour of K = 3 indicates a possible breakdown pattern associated with higher anisotropy.

V-4 Experiments on SQBD of Higher Anisotropy

As shown in the previous discussion, the higher the breakdown voltage, the larger will be the anisotropic effect produced with the configuration of Al(+) on p-type substrate. In order to achieve a higher breakdown voltage, we need only use an MOS capacitor with thicker oxide.

Experiments were performed on samples of 3000Å and 4000Å thermally grown SiO_2 on p-type substrates. Aluminum field plate of 200Å thickness and of 5×10^{-2} cm^2 area were vacuum deposited. The thin metal field plate provided enough electrical conductances but produced minimal interference with the heating contour from its heat capacity. Breakdown was induced at room temperature.

SEM micrographs of typical breakdown patterns on 3000Å-SiO_2 samples are shown in Fig. 5-4. The results for 4000Å-SiO_2 are shown in Fig. 5-5. When defects and weak spots are present, the breakdown voltage varies from one place to another across the sample, and this provides a very good opportunity to observe a variety of SQBD's as

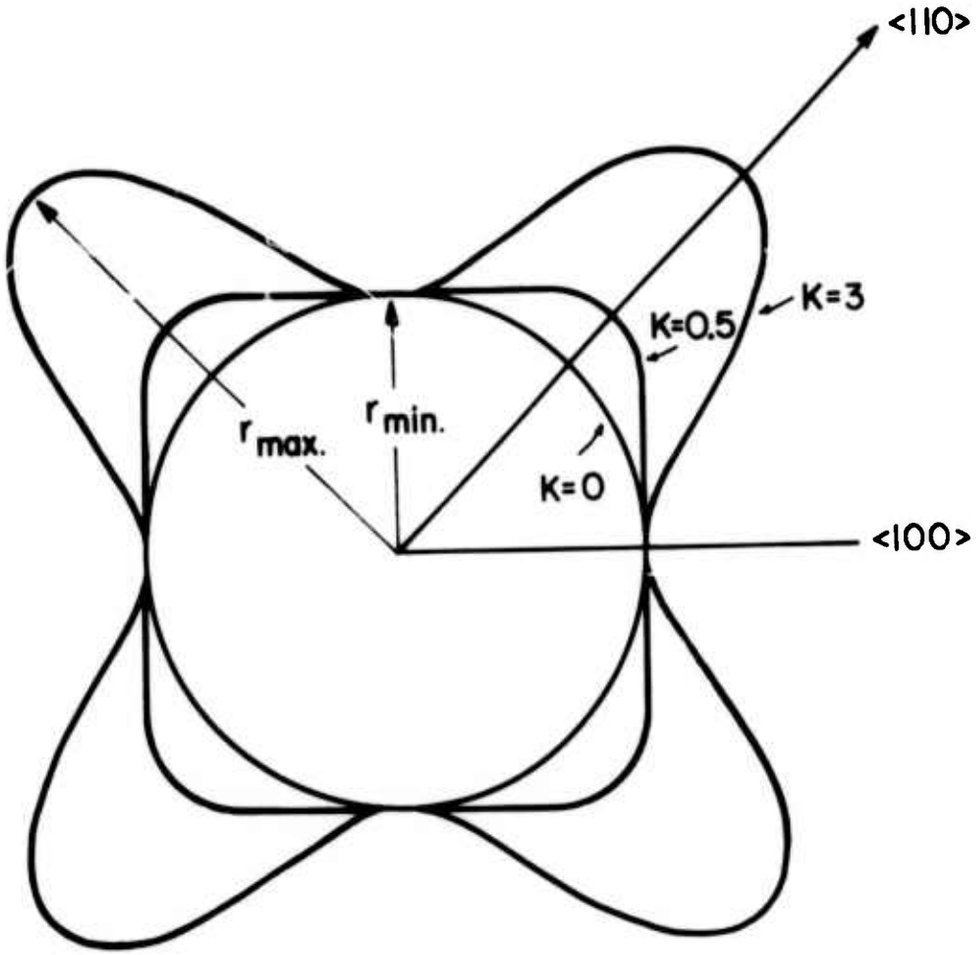

$$r(\theta) = (1 + K \sin^4 2\theta)^{1/2}$$

$$K = \frac{\sigma 110 - \sigma 100}{\sigma 100}$$

Fig. 5-3 Simplified model of constant joule heat contour as function of K.

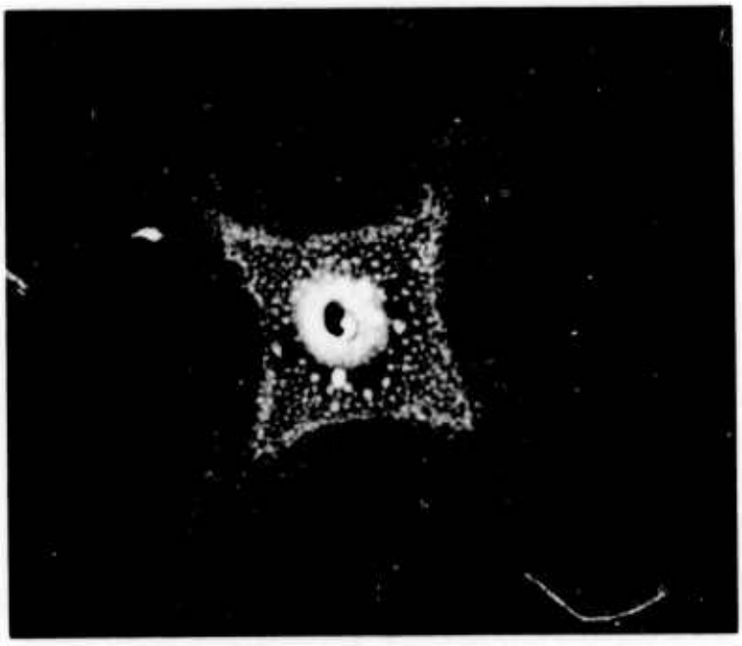

Fig. 5-4 SEM micrograph of anisotropic SQBD on (100) p-type substrate with Al(+). d_o= 3000A, V_b~230V, T= 300°K

X2,000

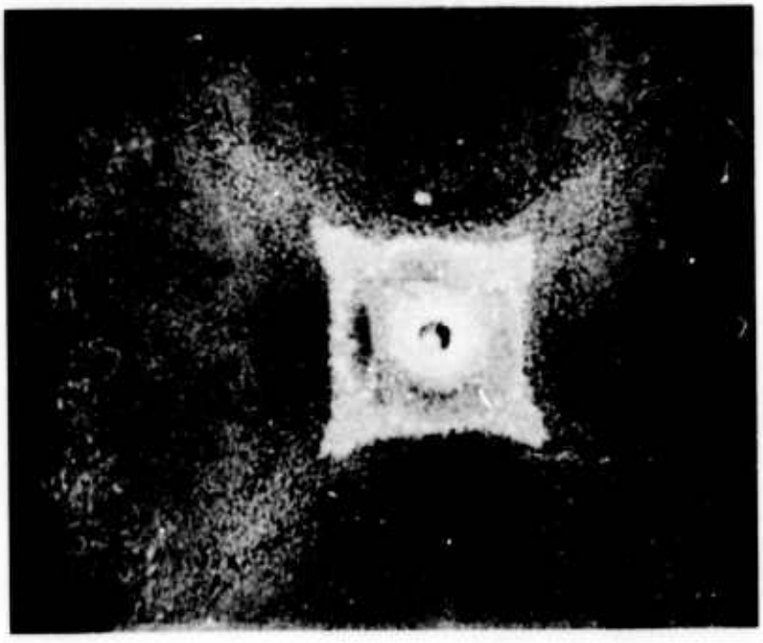

Fig. 5-5 SEM micrograph of anisotropic SQBD on (100) p-type substrate with Al(+). d_o= 4000A, V_b~280V, T= 300°K

X2,000

the applied voltage is gradually increased. Such patterns are shown in Figs. 5-6 and 5-7. The evolution of shape can best be seen in Fig. 5-7, in which 3 SQBD's occur, apparently on a scratch on the field plate, at different voltage levels: 170V, 200V, 230V for the round, square and stellar shapes respectively. This particular picture does indicate clearly that the shape is controlled by the field-dependent anisotropy as was mentioned in Section V-3.

An interesting point is that the breakdown spots for the thicker oxides do not show as clear a boundary between the remaining portion of the metal gate and the breakdown region as was seen in Fig. 4-6. This may be caused by the heat absorbed by the larger mass of the thicker oxide, or it may be caused by the thinner metal film. There are different hues of color in each SQBD as indicated in Fig. 5-8, corresponding to Figs. 5-4 and 5-5. If one assumes that the exposed insulator is entirely SiO_2, the colors would indicate that the oxide here is thicker than the bare oxide outside the metallization. A possible explanation is that part of the Al gate diffuses into the SiO_2 during the breakdown process to form some Al_2O_3. Since the index of refraction is higher for Al_2O_3 than for SiO_2, the combined layer of Al_2O_3 and SiO_2 would seem to be thicker, as judged on the basis of SiO_2 colors, than a layer of SiO_2 of the same total thickness.

Another experiment was done on samples of 1000Å SiO_2 on (100) p-substrates, with 200Å Al field plates of 5×10^{-2} cm^2 area. Only round shapes were seen, as in Fig. 5-9. Breakdown required only about 60V, which is too small to produce anisotropic effects.

Samples of (111) p-substrates were also tried. After breakdown on samples of 2000Å and 3000Å thick oxide at either 300°K and 100°K, no anisotropy was observed, presumably because of the almost equal conductivities along the <110> and <111> directions in the (111) plane, even at high fields.

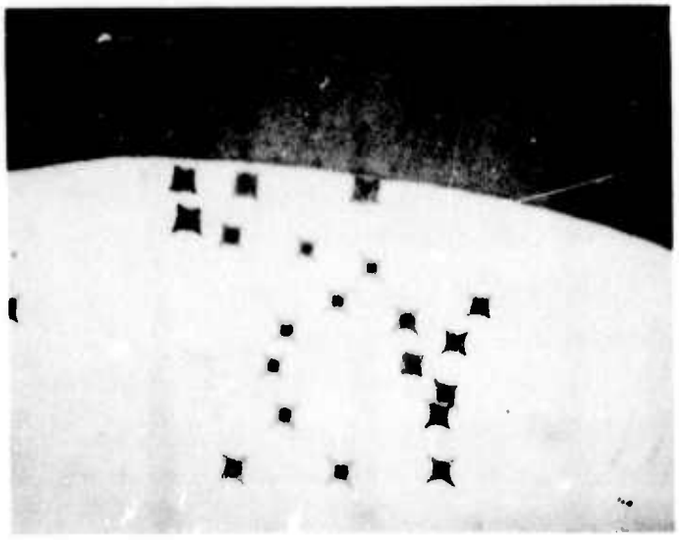

Fig. 5-6 Optical micrograph of anisotropic SQBD's on (100) p-type substrate with Al(+). d_o= 4000Å, V_b from 200V to 280V, T= 300 °K
X120

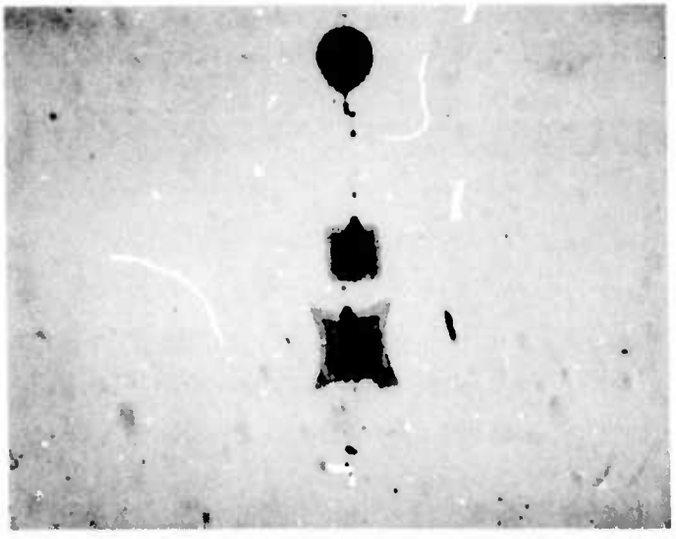

Fig. 5-7 Optical micrograph of SQBD's on scrtch on (100) p-type substrate with Al(+). d_o= 4000Å, V_b~170V (round), ~200V (square), ~230V (stellar), T= 300°K
X480

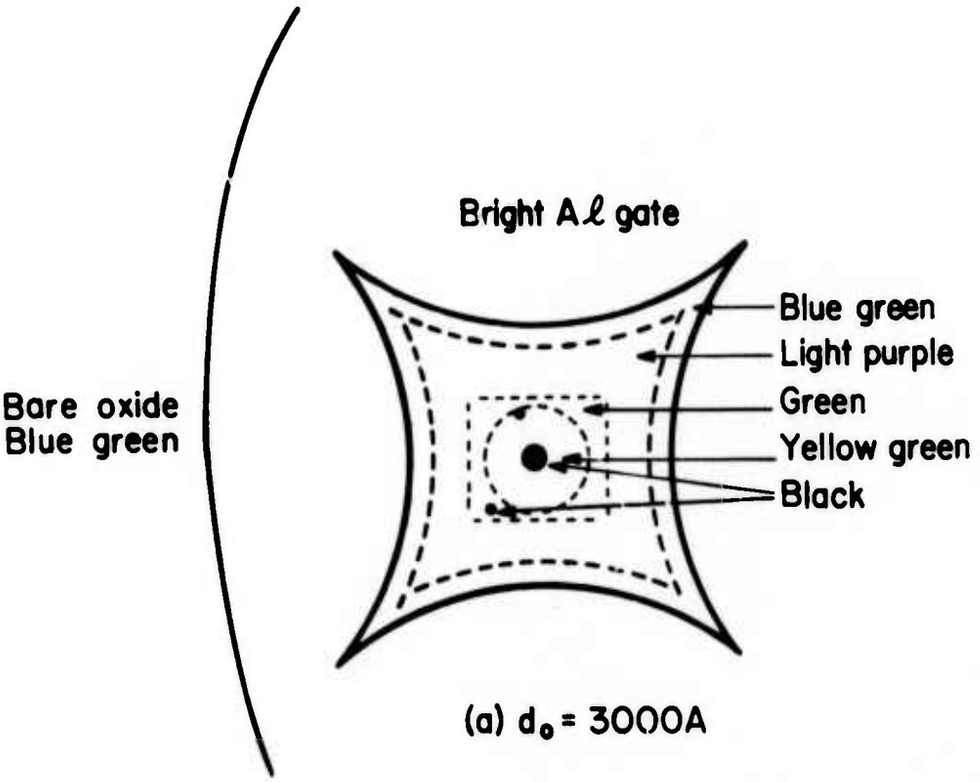

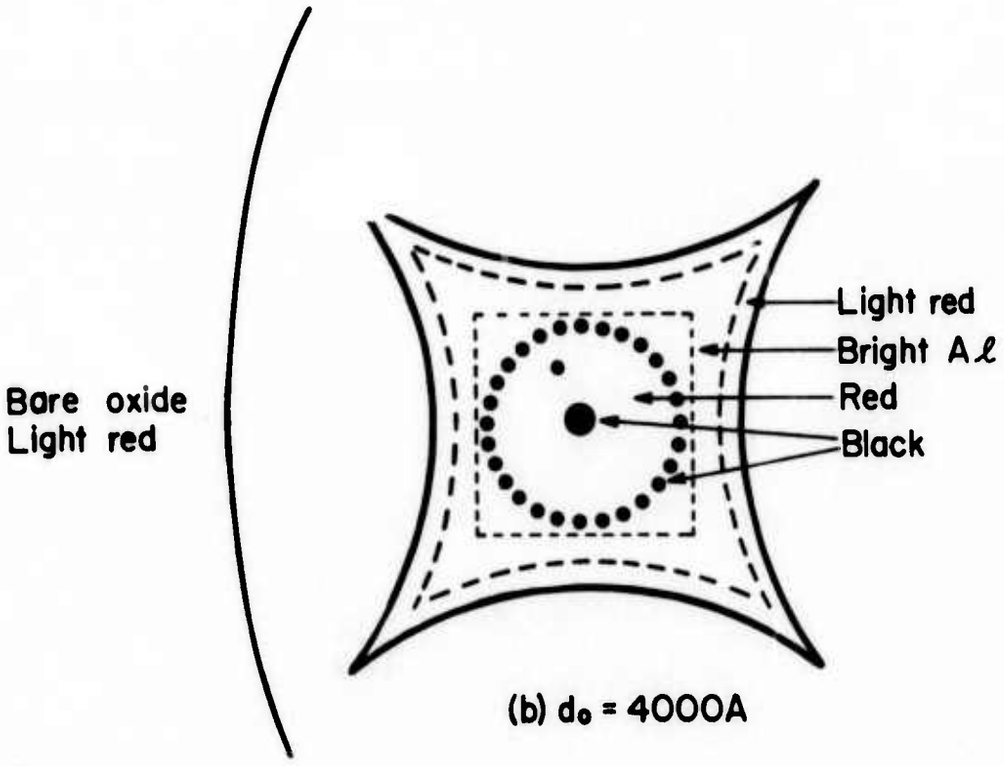

Fig. 5-8 Color diagrams corresponding to (a) Fig. 5-4 and (b) Fig. 5-5.

Fig. 5-9 Optical micrograph of SQBD's on p-type substrate with Al(+). d_o= 1000Å, V_b~60V, T= 300 °K
X480

V-5 Summary and Discussion

In this chapter, a new kind of anisotropic breakdown is studied on Al-SiO_2-Si structures. The development of this study begins with the square breakdown observed at 100°K on Al-SiO_2-p (100) Si with 2500Å thick SiO_2, using a positive polarity on the field plate. A simple schematic model was constructed, based on the anisotropy of hot electron conductivity in silicon, which explained the observed square breakdown and also predicted star-shaped breakdown patterns under conditions of larger breakdown voltage -- a prediction verified by experiments performed on thicker oxides.

Our choice of $f(\theta)$ gave us the requisite four-fold symmetry but was otherwise somewhat arbitrary. Thus the star shape depicted in Fig. 5-3 is, not unexpectedly, somewhat different from the actual shapes shown in Figs. 5-4 and 5-5. The reason for choosing a simple analytical function for $f(\theta)$ is that existing experimental data on the anisotropy of hot-electron conductivity are not sufficient to construct a complete field-dependent conductivity tensor which would be necessary for a more exact analysis.

However, the model does yield a radius ratio of

$$r_{max}/r_{min} = (\sigma_{110}/\sigma_{100})^{1/2}$$

In Figs. 5-4 and 5-5, measurements of the outer regions of the stellar shapes show that

$$r_{max}/r_{min} \sim 2$$

from which

$$(\sigma_{110}/\sigma_{100})^{1/2} \sim 2 \quad , \quad \sigma_{110}/\sigma_{100} \sim 4$$

This ratio is too large compared with that shown in references 24, 25, and 26, in which the ratio hardly exceeds 2.

There are at least two major reasons for this: (1) The data shown in references 24, 25, and 26 give the conductivity for bulk n-silicon. As is known from studies of MOS transistors, the conductivity of an inversion layer must be treated differently because of its 2-dimensional character. It is possible that only four constant energy ellipsoids, rather than six, are involved in the transport phenomena in the inversion layer. Interface scattering is different from bulk scattering, and lateral nonuniformities may well play a major role. Thus, bulk data are not directly applicable to the inversion layer. (2) Secondly, the equation is true only under the assumption that the electric field is radial and varies as 1/r. A more realistic analysis which would take into account the nonlinearities, anisotropies, and the various couplings would, unfortunately, be extremely formidable and would require the solution of a set of time dependent, nonlinear, inhomogeneous partial differential equations.

The SQBD's on samples of different oxide thicknesses and field-plate areas provide a good opportunity to check the dependence of breakdown area where the metal disappeared upon discharge of the capacitive energy. As in Equation (1-6), assuming complete discharge:

$$\int_0^\infty p \, dt = 1/2 \; C \; V_b^2$$

The quantitative comparison is made by comparing the ratio of damaged field-plate area to the total discharged energy for different samples and normalizing the ratio for the SQBD in Fig. 4-6(a) to unity.

The results are shown in the following table:

Sample	Damaged Area in Field Plate	Normalized Ratio
1. In Fig. 4-6(a) d_o = 2500Å A = 1.26×10^{-2} cm^2 V_b = 190V	$\sim (10\mu)^2$	1 (Arbitrary Reference)
2. In Fig. 5-4 d_o = 3000Å A = 5×10^{-2} cm^2 $V_b \sim$ 230V	$\sim (20\mu)^2$	0.81
3. In Fig. 5-7 (square) d_o = 4000Å A = 5×10^{-2} cm^2 $V_b \sim$ 200V	$\sim (16\mu)^2$	0.92
4. In Fig. 5-9 d_o = 1000Å A = 5×10^{-2} cm^2 $V_b \sim$ 60V	$\sim \pi(\frac{10\mu}{2})^2$	0.8

These ratios are very close to unity,i.e., the area of field-plate damage is very nearly proportional to the magnitude of the discharge energy.

Furthermore, the results of this comparison indicate clearly that the anisotropic SQBD's are not caused by anisotropic defects at the Si-SiO_2 interface, for the damaged area of the field plate in the anisotropic SQBD does vary as the geometrical area of the capacitor for a given SiO_2 thickness. If the anisotropic damage to the field plate reflected the anisotropic defects at the interface, the damage would not show this proportionality to the physical dimensions of the MOS structure.

CHAPTER VI

EXPERIMENTAL INVESTIGATIONS OF THE BREAKDOWN-INITIATING MECHANISM IN Al-SiO_2-Si STRUCTURES

In this chapter are described the results of electrical measurements which were designed to study experimentally the pre-breakdown conduction mechanisms in SiO_2 and associated high field instabilities in Al-SiO_2-Si structures. Emphasis will be on the instabilities which occur at electric field intensities below those at which a continuous occurrence of SQBD is observed (as shown in Fig. 4-11, designated with dashed-line and arrow). In such a high field region, the breakdown events are close to the intrinsic property of the Al-SiO_2-Si structure. Therefore, the results of electrical measurements, which supposedly represent the characteristics of the whole sample, can be related to the localized breakdown events. The instabilities can be related to the initiation of breakdown, i.e., the breakdown events can be treated as local fluctuations of instabilities. The self-quenching technique is used to eliminate the weak spots so that the magnitude of the field may approach the "intrinsic" breakdown field region without the occurrence of shorting.

In order to prevent possible interference by sodium ions, some of the experiments were performed at 100°K. However, the effects of sample temperature on breakdown were also studied.

VI-1 Steady-State Conduction in SiO_2

When a voltage is applied across the metal field plate and the silicon substrate, most of the voltage will finally drop across the SiO_2. The steady-state current through the SiO_2 can hardly be detected until the field exceeds about 6×10^6 V/cm. The transient current that flows immediately after the application of bias usually is about 2 or 3 orders of magnitude larger than the steady-state value. The physical mechanism of transient current has been studied and discussed by Osburn and Weitzman[15] and will not be discussed here.

The steady-state current was measured as a function of electric field intensity on samples with n- and p-type substrates and with both polarities of applied voltage. Typical procedures were used to achieve steady state: The sample was first biased to a field of 6×10^6 V/cm, for about 15-20 hours and then the current was measured one hour after each increment of applied bias. The applied field is cycled upward and downward to assure that the current is in steady state and reproducible. The same measurements were also carried out on different dots to check the reproducibility of the result.

The results of these measurements serve three functions: (1) to study the J-$\mathcal{E}$ characteristics per se, (2) to check for the presence of any excessive current as compared to the reproducible J-$\mathcal{E}$ characteristics and thus guard against anomalous conduction due to gross defects; in this case the data must be discarded, and (3) to detect any reproducible deviation or unstable current at very high fields.

First of all, the sign of the current carriers in SiO_2 can be identified in the following way:

After the sample is cleared of weak spots, the sample is biased at 100°K with such polarity that the silicon substrate is in the inversion condition. The the I-V characteristics and C-V curves are measured as functions of illumination on the sample with an ordinary incandescent lamp.

The results are presented in Fig. 6-1 for field plate positive on p-type substrate and Fig. 6-2 for field plate negative on n-type substrate.

In Fig. 6-1, both the I-V and C-V curves show great dependence on illumination level. The current is greatly reduced when the light is blocked from the sample and the current returns immediately to a higher and saturated value when the illumination is restored. This saturated value of current is almost of the same magnitude as the current measured on a similar sample with an n-type

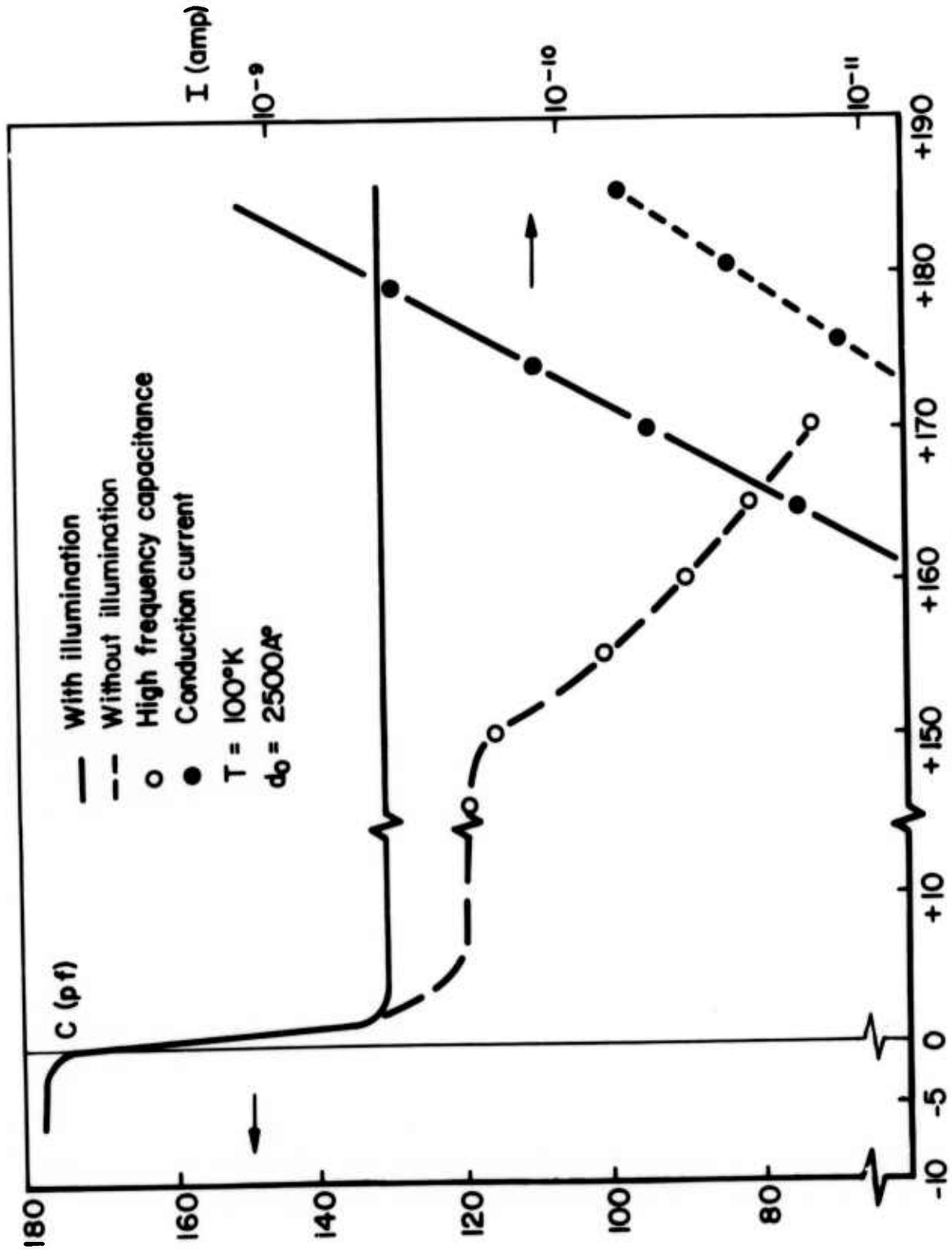

Fig. 6-1 I-V and C-V curves in high field with different illumination. (p-type)

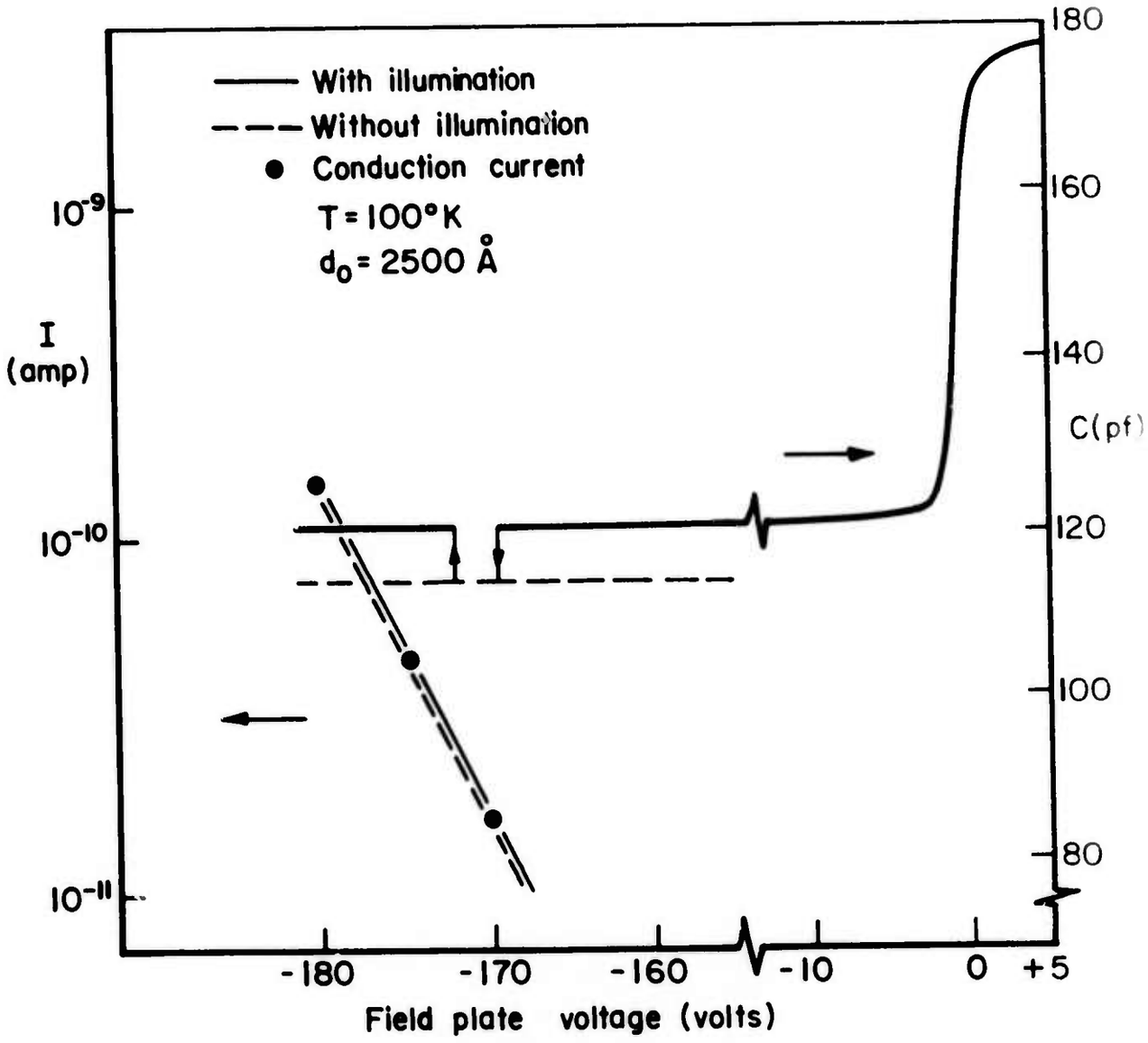

Fig. 6-2 I-V and C-V curves in high field with different illumination conditions. (n-type substrate)

substrate at the same field. The capacitance is measured before and after the light is blocked at different constant biasing voltages.

When the light is blocked, the high-frequency capacitance decreases immediately and decays for several minutes to reach its steady-state value. Illumination of the sample brings the capacitance up instantly. The onset voltage of the depletion region almost coincides with the field plate voltage, corresponding to 6×10^6 V/cm, at which current is detectable.

The evidence from these measurements is very clear that for Al field plate positively biased on p-type substrate samples, the current consists of electrons injected into SiO_2 from the n-type inversion layer in the p-type substrate. At low temperature and with no illumination, the generation rate of hole-electron pairs in the depletion region is so low that it can not supply enough electrons to sustain the n-inversion layer against the drain of electrons into the SiO_2 by the high field. Thus, the electric field will penetrate deeper into the substrate and widens the depletion region. The current injected into the SiO_2 is greatly reduced because of (1) the exhaustion of the available electrons in the inversion layer and (2) because of the reduction in the electric field in the oxide as a result of the increasing voltage drop in the deep depletion region of the substrate.

Eventually a balance is achieved between the increase in supply of generated electrons from the deep depletion region and the injection of electrons into the SiO_2, and the current will reach a steady state; otherwise an avalanche process in the deep depletion region will take over as the main supply of electrons needed. For the same (positive) field-plate polarity on samples with n-type substrates, it is expected that electrons injected from the substrate will still be the current carriers in the SiO_2.

In Fig. 6-2, with an n-type substrate and the Al field plate negatively biased, the I-V and C-V characteristics remain very nearly the same between the dark condition and illumination with incandescent light. Using reasoning similar to that of the

preceding paragraph, it is evident that the current is not due to holes injected into the SiO_2; insteady, it still consists of electrons into the substrate from the oxide, presumably after injection from the metal field plate. Furthermore, the arriving electrons obviously do not recombine with the holes in the p-type inversion layer in the substrate. The p-type inversion layer is always sustained without resulting in deep depletion region in the substrate. This is not surprising, for the electrons entering the silicon substrate have a kinetic energy at least as large as the barrier height between the conduction bands of $Si-SiO_2$ ($\sim$ 3.1 ev), and the chance for these entering electrons to recombine with the holes in the thin (about 10Å) p-inversion layer should be very slight. One can expect that for a p-type substrate with negative Al polarity, the current is also due to electrons injected from the Al field plate.

The above results not only provide a quick identification of the current carriers through SiO_2 in $Al-SiO_2-Si$ structures for each of the two field plate polarities but also are able to justify the SQBD studies in Chapters IV and V, in which field-plate-positive SQBD's on p-type substrate and field-plate-negative SQBD's on n-type substrate were always studied under illumination to avoid the complications due to deep depletion and avalanche processes in the substrates. In other words, the samples were illuminated to prevent breakdown in the deep depletion region, which may interfere with the breakdown of the SiO_2, and also to minimize the voltage drop in the substrate depletion region, so that the actual voltage drop in the oxide can be approximated to the external applied voltage with reasonable accuracy.

The resultant steady state $J-\mathcal{E}$ characteristics for both field polarities is shown in Fig. 6-3 for field intensities in the range $6-8 \times 10^6$ V/cm. Essentially the same results were obtained for both types of substrate. In the small range of applied fields used here, the current density varies from 10^{-9} to 10^{-6} amp/cm^2 and log J has an almost linear relation with electric field except in the

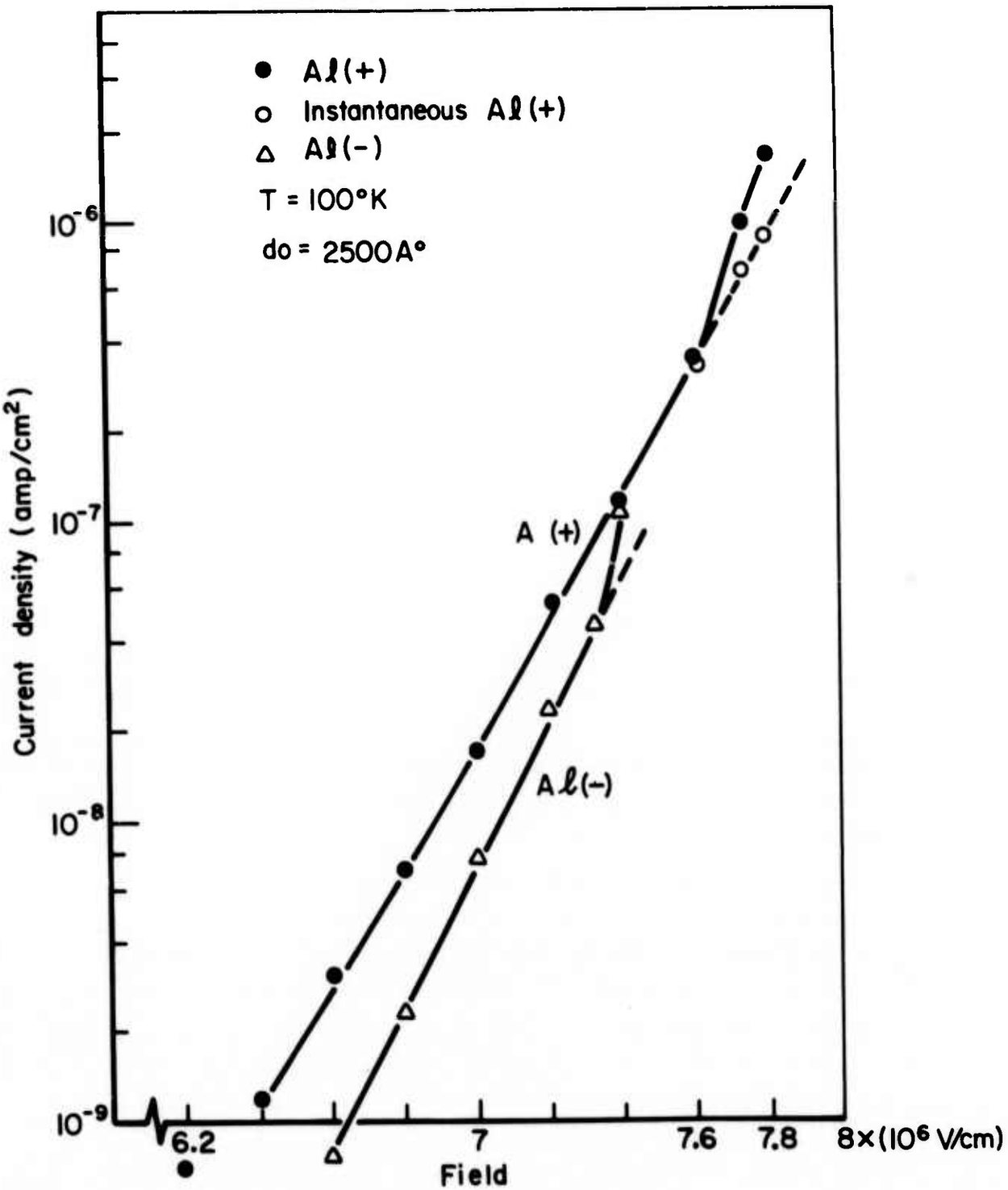

Fig. 6-3 J-$\mathcal{E}$ characteristics of conduction in SiO_2. Essentially the same results are obtained for both types of substrates.

very high field region where the current density tends to deviate from the linearity just before continuous breakdown events begin to errupt. This deviation, or instability, will be discussed in the following sections.

The main current conduction mechanism, in thermally grown SiO_2 which results in the "linear" portion of J-$\mathcal{E}$ characteristics, was first studied by Lenzlinger and Snow,[11] then by Osburn and Weitzman,[15] and recently by Weinberg[27] using corona charging. In their results the conduction mechanism is believed to be electron tunneling into the conduction band of SiO_2 through a triangular barrier and to follow the Fowler-Nordheim relation expressed in the following equation:

$$J_{FN} = C\mathcal{E}^2 [f(T)/t^2(y)] \exp[-(\mathcal{E}_o/\mathcal{E}) \cdot v(y)] \qquad (6\text{-}1)$$

here

$$C = \frac{q^3 \mathcal{E}^2 m_o}{8\pi h \phi m^*}$$

$$\mathcal{E}_o = \frac{-4(2m^*)^{1/2} \phi^{3/2}}{3\hbar q} \quad ,$$

and

$$f(T) = \frac{\pi ckT}{\sin \pi ckT}$$

f(T) is a temperature correction factor of the order of unit, in which $c = 2(2m^*\phi)^{1/2}\, t(y)/\hbar q\mathcal{E}$. t(y) and v(y) are two correction factors that take into account the effect of the image force on the barrier. Both are tabulated elliptical integrals and can be found in reference 28 as functions of a normalized image-force barrier-lowering parameter y:

$$y = (1/\phi)\ (q^3\mathcal{E}/4\pi\varepsilon)^{1/2}$$

here

q = charge of an electron

ϕ = barrier height for electron tunneling

$h, \hbar$ = Planck's constant

ε = dielectric permittivity of the thermally grown SiO_2

$\mathcal{E}$ = electric field intensity

k = Boltzmann's constant

m^* = the effective mass of an electron in the forbidden gap of the SiO_2

m_o = the free electronic mass.

Since the correction factors t(y), F(t) and v(y) are very close to unity, for simplicity the Fowler-Nordheim Equation (6-1) can be rewritten as:

$$J_{FN} = C \mathcal{E}^2 \exp(-\mathcal{E}_o/\mathcal{E}) \qquad (6\text{-}2)$$

The linear portion of Fig. 6-3 can be replotted in a Fowler-Nordheim plot, log $(J/\mathcal{E}^2)$ vs. $(1/\mathcal{E})$ as in Fig. 6-4. From this $\mathcal{E}_o$ can be calculated from the slopes of the two (still linear) lines. For a positive Al field plate and electrons tunneling from the substrate we obtain

$$\mathcal{E}_o,Si = 2.32 \times 10^8 \text{ V/cm}$$

For the Al field plate baised negatively and electrons tunneling from the Al field plate,

$$\mathcal{E}_o,Al = 2.70 \times 10^8 \text{ V/cm}$$

By putting the numerical values of $\hbar$ and q into $\mathcal{E}_o$,Si and $\mathcal{E}_o$,Al, we find

$$(m_{Si}^*/m_o)^{1/2} \ (\phi Si/q)^{3/2} = 3.4 \ (\text{volt})^{3/2}$$

$$(m_{Al}^*/m_o)^{1/2} \ (\phi Al/q)^{3/2} = 3.95 \ (\text{volt})^{3/2}$$

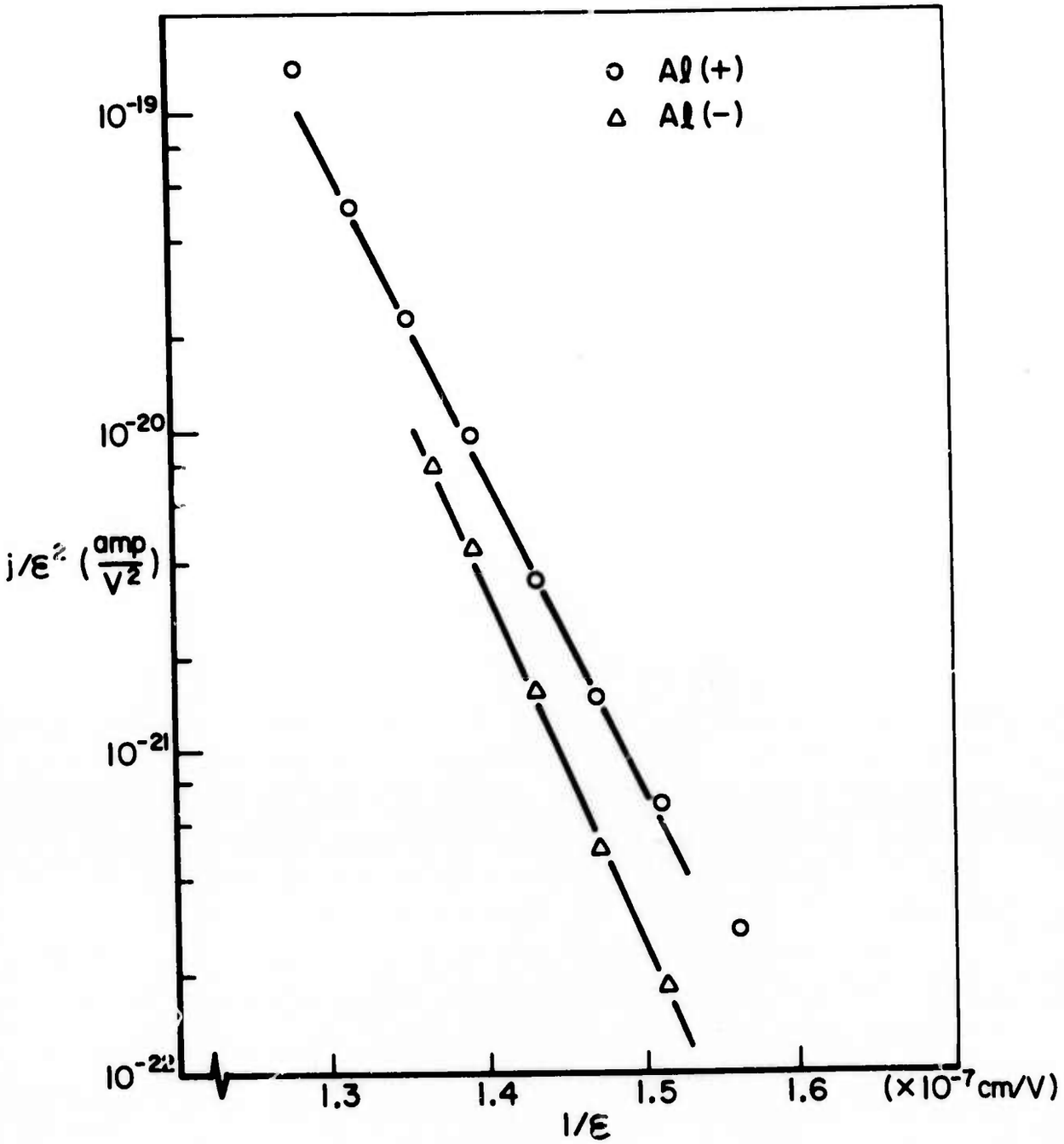

Fig. 6-4 Fowler-Nordheim plot of j-$\mathcal{E}$ characteristics. (Replotted from Fig. 6-3)

By using the barrier heights $\phi_{Si}/q = 3.1$ ev and $\phi_{Al}/q = 3.25$ ev, we obtain

$$m^*_{Si}/m_o = 0.38$$

$$m^*_{Al}/m_o = 0.46$$

These values are in reasonably good agreement with those obtained in previous studies.

Comparing the magnitude of the current density with the results of previous studies, we find our current densities for electron tunneling from Si substrate to be comparable with the values obtained by Osburn et. al. and Weinberg; however, the current densities for electrons tunneling from the Al field plate are about a decade higher than those reported by Osburn et. al.

VI-2 Current Instability and Positive Charge Storage in SiO_2

In Fig. 6-3, the logarithm of the current density is found to deviate upward from a linear relationship with the field intensity. This is the result of an instability which is always observed in very high fields as the current tends to increase with time when the (constant) applied field is close to the value at which continuous breakdown events are about to occur. The instability occurs at 7.6×10^6 V/cm when the field plate is positively biased and at 7.3×10^6 V/cm when the field plate is negatively biased.

The current instability is found to be very reproducible and the current is found to be proportional to the area of the field plate, thus indicating that the instability occurs under the entire field plate. Figure 6-5(a) shows a series of current instabilities with the applied voltage as a parameter. Each instability was obtained on a fresh sample. It is clear that the instability is more prominent at higher applied voltages. Breakdown events do errupt occasionally (as shown by the impulse) without disrupting the main trend of the current. In Fig. 6-5(b), the C-V curves, measured after the samples are biased at the indicated applied voltage

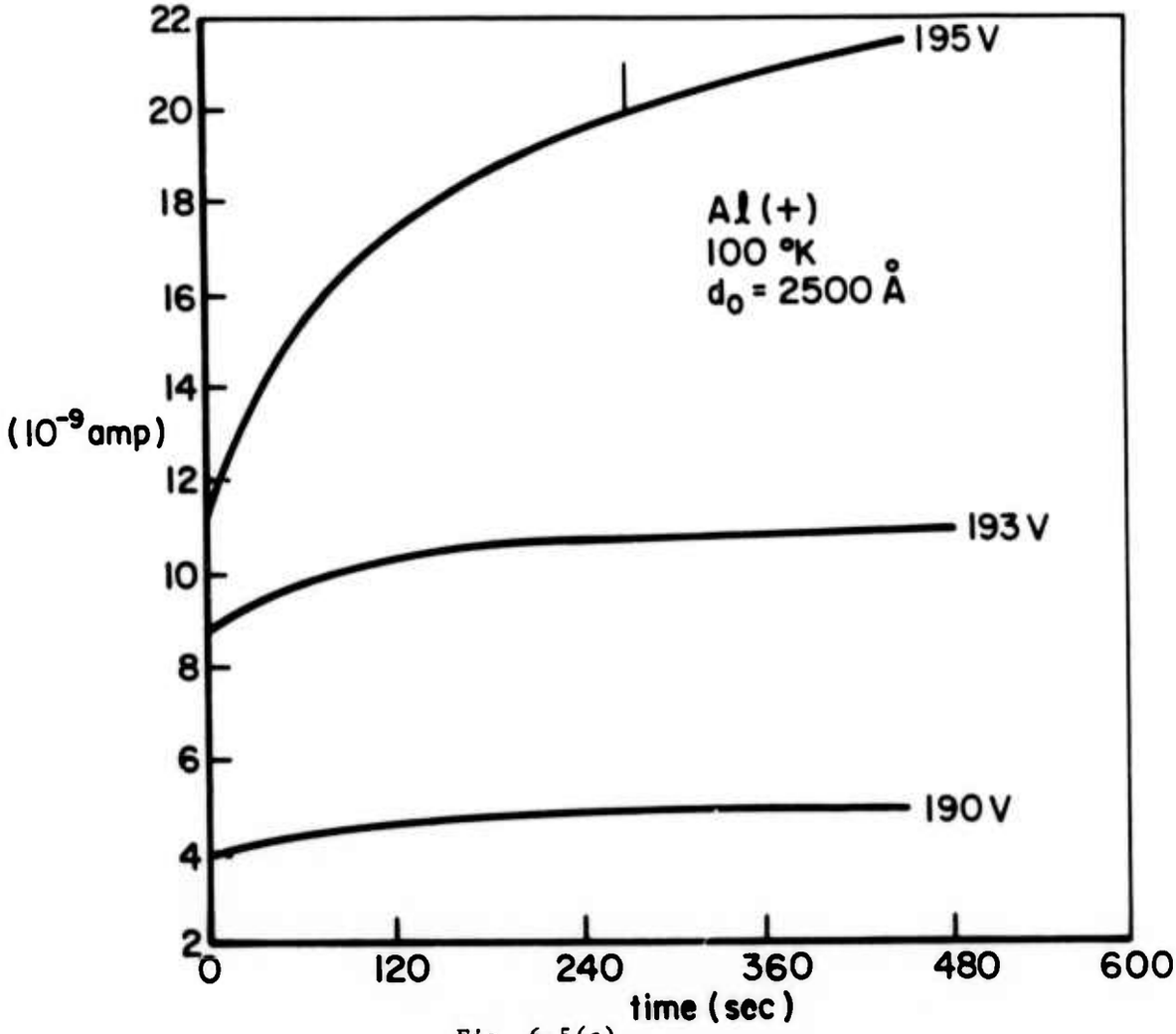

Fig. 6-5(a)

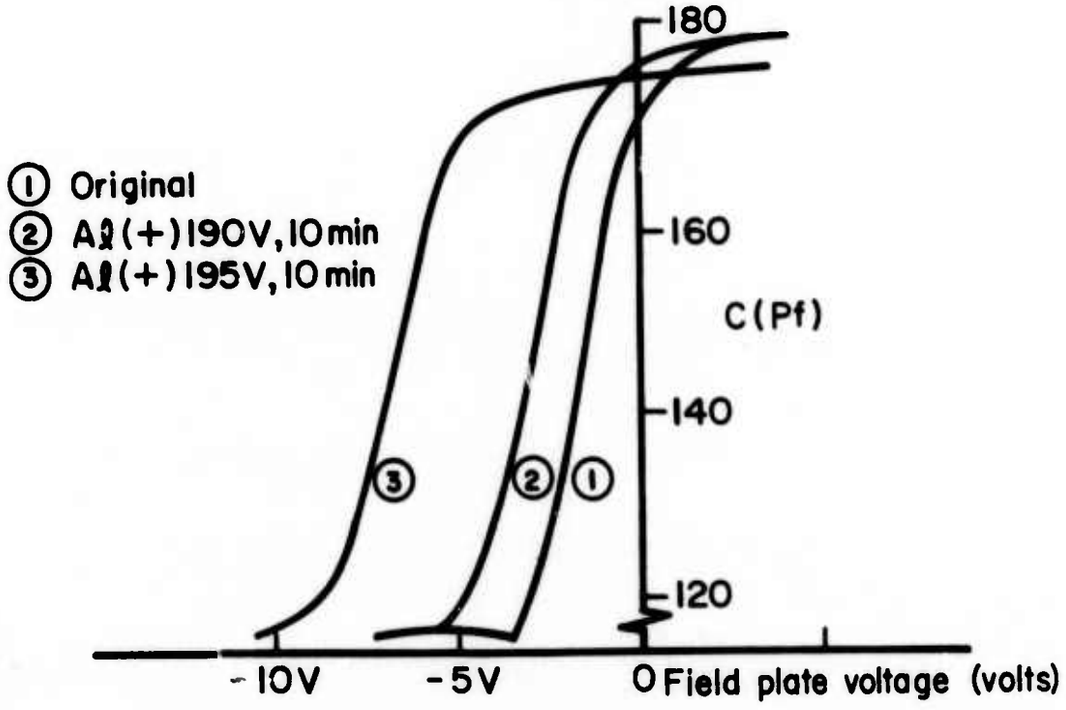

Fig. 6-5 (a) Current instability and (b) associated flatband shifts after 10-minute bias.

for about 10 minutes, indicate negative flatband shifts which indicate the storage of positive space charge in the oxide or at the interface. The cause of this may be sodium ions which migrate to the $Si-SiO_2$ interface under the influence of the high field or the trapping of holes generated in the silicon bulk, or the trapping of holes which have tunneled from the positively biased field plate (we consider this unlikely), or the positive charging of defect states in the SiO_2 as a result of some high-field ionization process. By comparing Figs. 6-5(a) and 6-5(b), the correlation between the current instability and the positive charging of the SiO_2 is obvious: more positive charges correspond to a greater current instability. Since the current through the SiO_2 is primarily the result of Fowler-Nordheim tunneling as was described in the last section, the current is very sensitive to the magnitude of the electric field near the tunneling contact. The presence of positive charges near the electron tunneling contact at the $Si-SiO_2$ interface will enhance the electric field at the tunneling contact and consequently will enhance the tunneling current. The enhancement of electric field and the flatband voltage shift due to the presence of positive charges can be expressed as (neglecting work-function differences):

$$V_{FB} = -\frac{1}{C_o} \int_o^{d_o} \frac{x}{d_o} \rho(x)\, dx \tag{6-3}$$

$$\mathcal{E}_c = \frac{V_a}{d_o} + \frac{1}{\varepsilon} \int_o^{d_o} \rho(x) \frac{x}{d_o} dx = \frac{V_a - V_{FB}}{d_o} \tag{6-4}$$

where $\rho(x)$ is the distribution of positive charges with distance measured from the field plate,

V_a is the field-plate voltage,

$\mathcal{E}_c$ is the electric field at the tunneling contact (the $Si-SiO_2$ interface),

C_o is the oxide capacitance per unit area = ε/d_o,

ε is the dielectric permittivity of the oxide,

d_o is the oxide thickness.

From external measurements, it is not possible to find out the exact distribution, $\rho(x)$, of the positive space charge in the SiO_2. We note, however, that with the Al field plate negatively biased, same instability is observed, but there is no significant flatband shift associated with the instability, hence it is reasonable to assume that the positive charges are near the electron tunneling contact, i.e., near the SiO_2-Si interface with positive field plate polarity and near the SiO_2-Al interface with negative field plate polarity. In the later case, the positive space charge can hardly be detected as a flatband shift in C-V measurements.

The nature of the positive space charge is very important because this charge is closely related to the current instability and to the breakdown-initiating mechanism.

In spite of the low temperature at which these particular experiments are performed, sodium ions or other ions may still be mobile under the influence of very high electric fields. Bias-temperature-stress was used on both samples that displayed negative flatband shifts due to previous exposure to high fields and also on fresh samples.

After a negative flatband shift was observed, the sample was annealed at 300°C for 2 hours with positive bias $\sim 2 \times 10^6$ V/cm on the field plate so that possible ions will be kept at the SiO_2-Si interface and can be detected as flatband shifts after sample is cooled down to 300°K. The actual experimental result showed that the negative flatband shift disappeared after this bias-temperature-stress treatment. Fresh samples subjected to the same bias-temperature-stress treatment showed negligible flatband voltage shift. This indicates that the sodium ion contamination is low and the positive charges were not sodium ions.

If the electric field is reduced below the value that produces instability, instability after the negative flatband shift is seen in high fields: the current does not return to its previous steady-state level but instead moves to a magnitude which is larger than its previous steady-state level and then decays slowly to the previous steady-state level. The negative flatband shift decreases

accordingly. The disappearance of negative flatband shifts upon lowering the applied voltage is shown in Fig. 6-6(a) for p-type substrate and Fig. 6-6(b) for n-type substrate. The hysteresis loops in the C-V curves might be due to generation via interface states. In this particular study, only flatband shifts are of major concern.

The interpretation of these reduced flatband shifts is that the process responsible for introducing the positive charges in SiO_2 can only occur above a certain threshold electric field. When the electric field is lowered below that threshold field, the process stops and the positive charges are still there enhancing the electron tunneling; however, the electrons tunneling into the SiO_2 gradually recombine with the positive charges and annihilate the positive charges. The electric field near the tunneling contact then gradually returns toward the nominal average electric field in oxide, i.e., the applied voltage divided by oxide thickness.

All of these arguments suggest that in the instability region both the generation and annihilation of positive charges are occurring and in the lower field region only positive charge annihilation takes place. The annihilation process not only manifests itself in the reduction of negative flatband shifts in lower field also can be perceived as the factor which contributes to the apparent saturation of the current instability shown in Fig. 6-5(a).

It appears also from this argument that the positive charges are of an electronic nature, i.e., they are introduced via an electronic process and can be annihilated via an electronic process. The electronic processes which can introduce positive charges in SiO_2 can be confined to impact ionization of defect states of the lattice or the tunneling of holes. Because of the low mobility of holes[29] and numerous trapping centers in SiO_2, holes introduced in SiO_2 can be trapped and can be detected in terms of C-V flatband shifts.

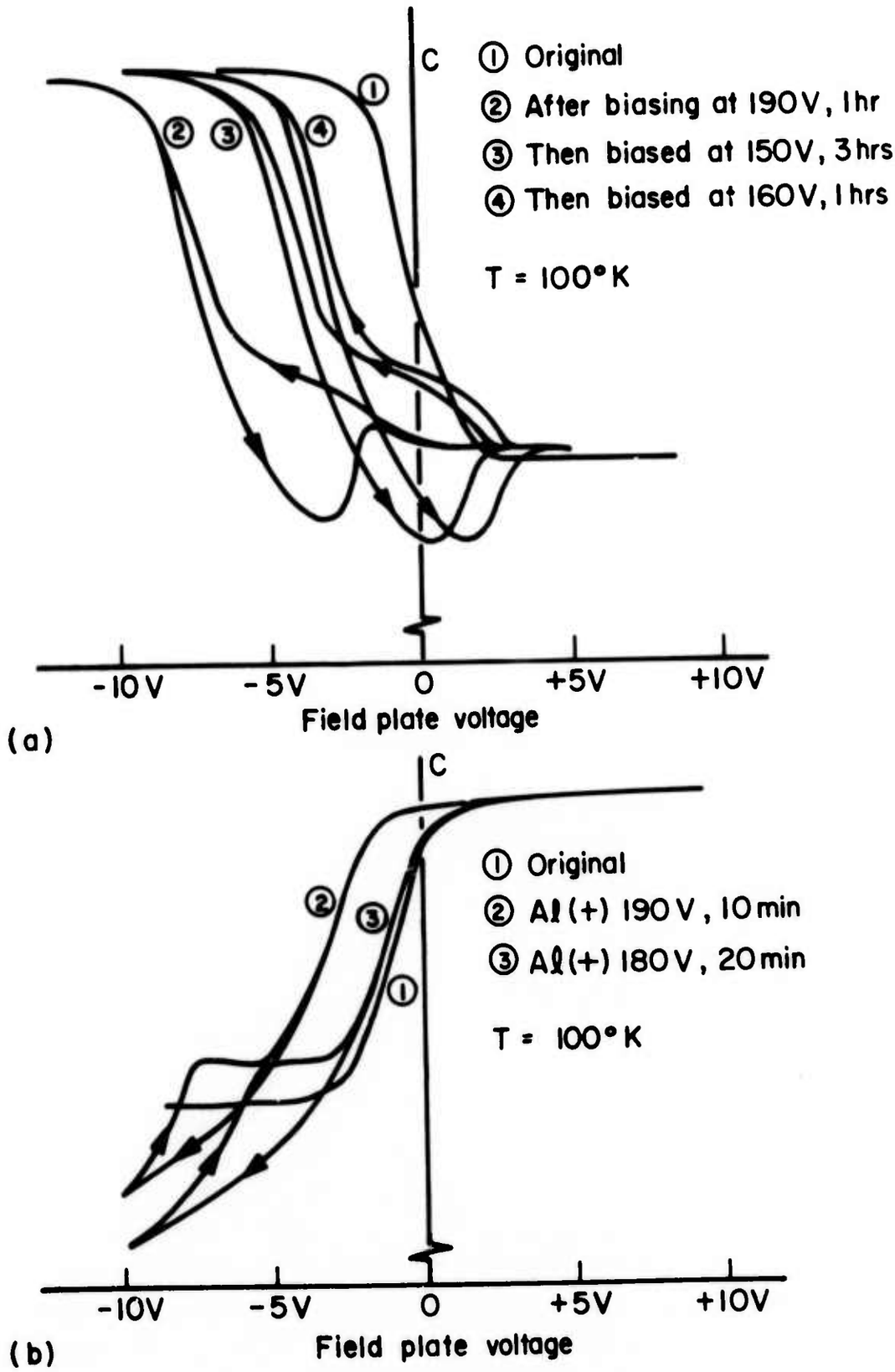

Fig. 6-6 Electronic annealing of positive charges (a) on p-type substrate and (b) on n-type substrate.

VI-3 Instability Associated With Low Temperature

Although the results shown in Fig. 6-5(a) and (b) were obtained when sample temperature was at 100°K, a current instability is also seen at room temperature. However bias-temperature-stress still does not show any sodium ion migration. Therefore the instabilities that occur at both 100°K and 300°K should be of the same nature.

The idea of cooling a sample while it is biased in a constant high field originates from the result, shown in Fig. 4-11, in which distribution of breakdown field tends to shift to lower field at 100°K compared with the distribution of breakdown fields at room temperature. However, the shift is very slight and may be caused simply by the variation from sample to sample. The result needs to be confirmed simply by changing the sample temperature while the sample is biased in a very high field to see if the breakdown events do increase or not when the temperature is being lowered.

Experimentally, the measuring procedure is to increase the applied voltage to such point that current instability can be seen at room temperature, then the voltage is kept constant and the current is monitored with a chart recorder while liquid nitrogen is poured into the sample chamber dewar. Temperature is measured at intervals with a thermocouple. In order to prevent any surface charge motion due to moisture, the sample is pre-baked at 75°C and the vacuum chamber is pumped down to 10^{-4} torr.

Figures 6-7 and 6-8, duplicated from the chart-recorder, show that the current increases as the sample temperature is lowered to about -70°C in a high field. The front portion, which shows current instability before cooling, is the same instability discussed in the last section. The spikes are the current impulses caused by self-quenched breakdowns. Since the current impulses do not interfere with the current instability or disrupt the increasing current, it is inferred that the current instability is not caused by any localized current leakage. This means the current instability produced by temperature-lowering is the property of the whole sample.

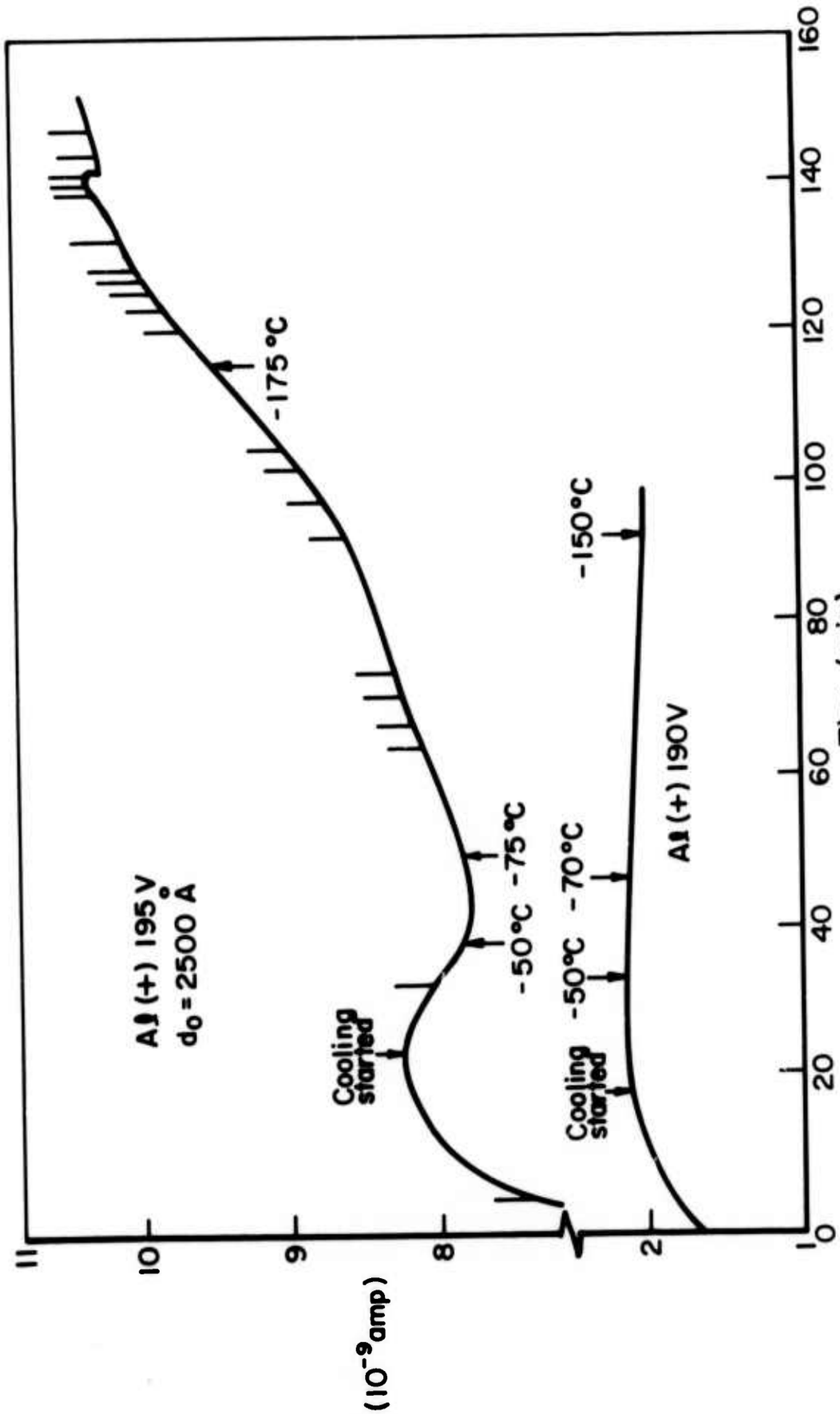

Fig. 6-7 Current instability and breakdown on lowering temperature.

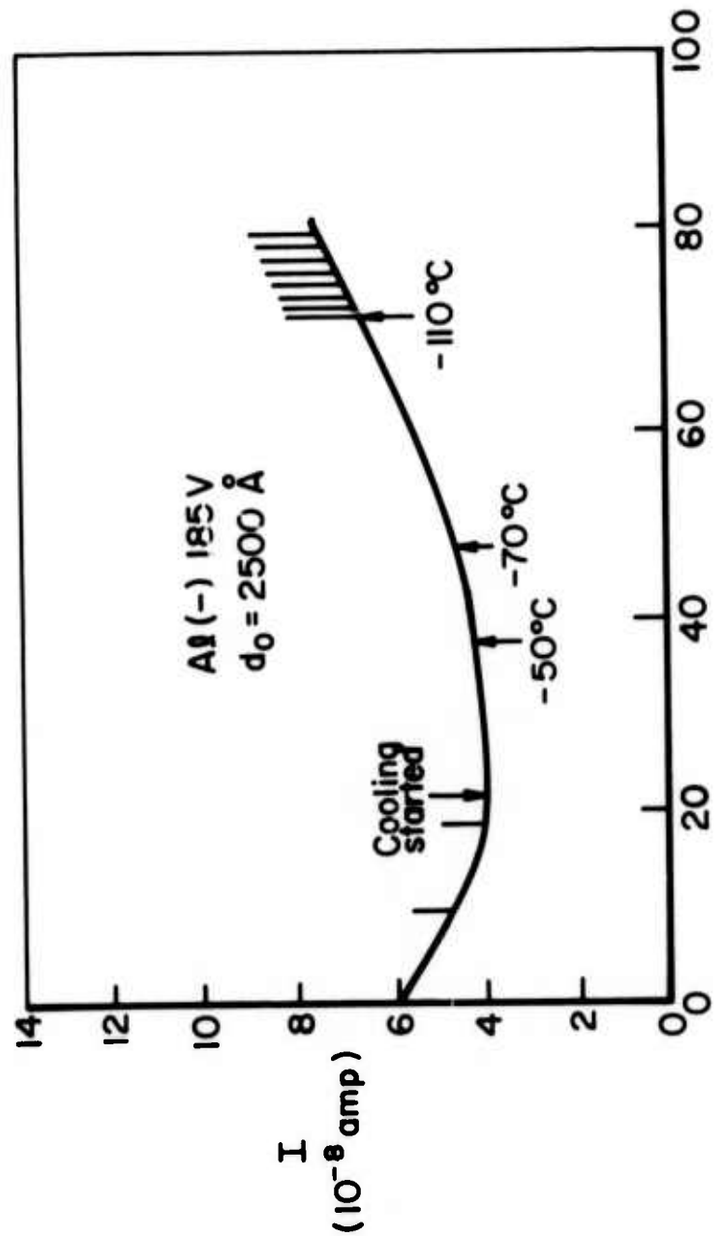

Fig. 6-8 Current instability and breakdown on lowering temperature.

In Fig. 6-7, the rate of breakdowns apparently increases as the current increases with lowering temperature while the applied voltage on the field plate is +195V, corresponding to 7.8×10^6 V/cm.

In Fig. 6-8 the breakdowns simply erupt continuously when the applied voltage corresponds to 7.4×10^6 V/cm, negative polarity on the field plate so that the applied voltage had to be removed to avoid too many damaging breakdowns. This particular result just confirms the results shown in Fig. 4-11(a) and (c). In Fig. 4-11(a), the breakdown events occur continuously at 7.6×10^6 V/cm at 300°K. In Fig. 4-11(c) the breakdown events erupt continuously at 7.4×10^6 V/cm at 100°K.

It is of interest to note that at lower fields, as in Fig. 6-7, when the applied voltage on field plate is +190V, no current increase is observed; instead, the current drops slowly, presumably dictated by the slight temperature dependence of the Fowler-Nordheim relation.

Other tests while cooling the sample when biased at a lower field were also conducted and showed no current instability.

The significance of these aresults are:

(1) Besides the current instability at constant temperature discussed in last section, this particular instability is associated with temperature lowering and high field.

(2) That this current instability is not seen when the applied field is not so high indicates that the current increase cannot be due to surface-charge flow, change in the sample geometrical structure, or a lowering of the tunneling barrier while the temperature is being reduced.

(3) Because the rate of breakdown increases as the current increases upon lowering of the temperature, it is clear that the instability is closely associated with the breakdown process.

(4) It is clear that the instability is not thermally initiated.

VI-4 Discussion of Current Instability and Modeling of Localized Breakdown

At this point, the results on the current instability can be summarized as follows:

(1) At a constant temperature, either 100°K and 300°K, a current instability occurs at very high applied fields, is probably associated with positive space charge introduced by an electronic process.

(2) At very high fields, a current instability occurs while the temperature is being lowered. The C-V curves always smear out at room temperature after high field stress. This temperature-dependent smear-out will be discussed in section VI-5. It becomes a major obstacle in studying the positive charging in the second kind of current instability.

However, since the second instability only occurs at very high fields, one may assume that its physical interpretation is the same as that for the first kind of instability, i.e., it is caused by the enhancement of tunneling field due to the presence of positive charges. It is likely that on lowering the temperature, more positive charges are generated or fewer are recombined; therefore, the enhancement of the tunneling field is greater at 100°K than at 300°K. No matter how the positive charges increase so that they enhance the electron tunneling current, they have had to be introduced into the SiO_2 at the first place.

A process which can account for both instabilities is impact-ionization. That is, as electrons tunnel into the SiO_2, they gain energy from the electric field and lose energy by collision with phonons or impurities. The energy they obtain between collisions is determined by the magnitude of the electric field and by the mean free path between collisions. If the field is high enough they may obtain enough kinetic energy to ionize the lattice or impurities on collision. At lower temperature, for the same field, the mean free path is increased so that electrons can gain a greater kinetic energy. Therefore, the impact process can account for both instabilities.

At constant temperature, the instability is due to impact ionization by energetic electrons gaining energy from the high field. At a constant high value of electric field intensity, the mean free path of electrons increases as the temperature is reduced, resulting in more impact ionization and greater instability.

When impact ionization creates electron-hole pairs, the electrons will be swept out of the SiO_2 because of their relatively high mobility[30] and because of the low density of electron trapping center in SiO_2.[31] Holes will be trapped near the Si-SiO_2 interface because of the relatively large density of hole trapping centers there. The holes accumulated near the interface will increase the electric field intensity and thus will exert positive feedback and enhance the electron tunneling.

Since the bandgap of SiO_2 is about 9eV,[32] an electron would have to travel about 100Å without any collision in order to gain such a large amount of kinetic energy. The probability for an electron to gain 9eV of kinetic energy in amorphous SiO_2 must be very slight. It has been proposed[15] that the current instability might be caused by impact ionization of defect states in the forbidden gap; thus the electrons would need less than 9eV of kinetic energy to produce ionization.

Since the transport properties of SiO_2 are not well understood at the present time, only a phenomenological model will be presented, as shown in Fig. 6-9, using impact ionization as the main mechanism of instability.

In this model, electrons tunnel into the SiO_2 according to the Fowler-Nordheim relation. Some of the electrons gain kinetic energies great enough to produce impact ionization. When electron-hole pairs are created, the electrons are swept out of the SiO_2 and the holes move to the tunneling contact under the influence of electric field and are trapped near the tunneling contact. The accumulation of trapped holes not only enhances the electric field for more electron tunneling but also increases the chance for electrons to recombine with the trapped holes. The current approaches a steady-state value as the hole generation and trapping is balanced

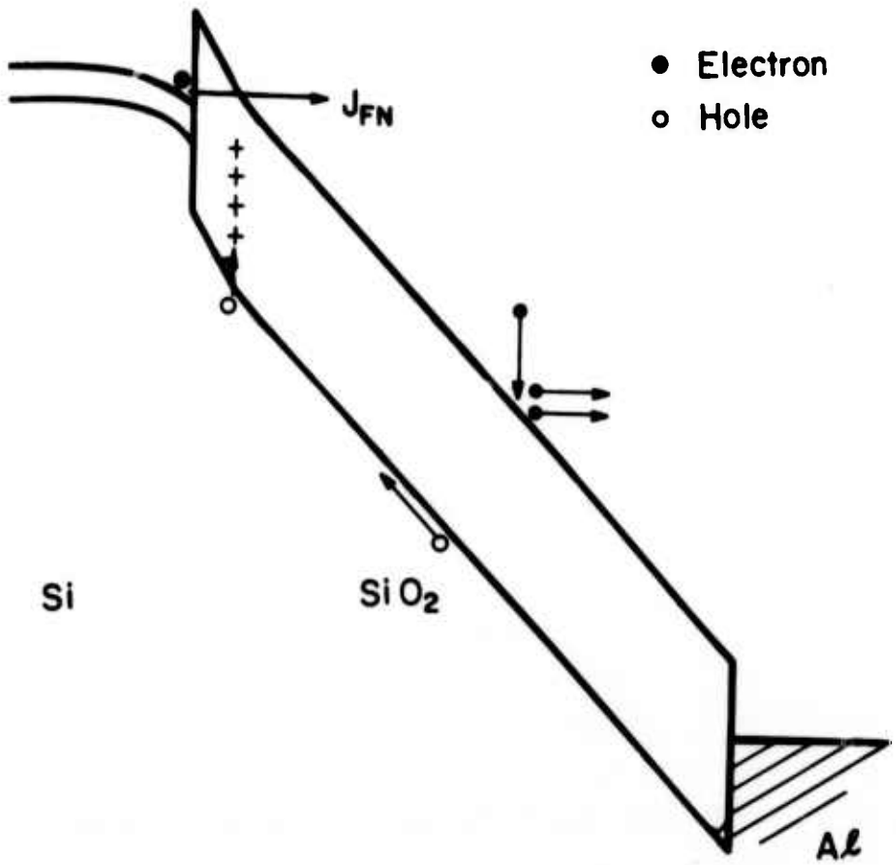

Fig. 6-9 Simple model for current instability and breakdown.
(not to scale)

by recombination with electrons.

This phenomenological model can be expressed as follows:

We assume that hole-electron pairs are produced by impact ionization at a rate proportional to the current density of injected electrons: $\alpha d_o J_{FN}$ hole-electron pairs per cm^2 of sample, where α is a function of the electric field intensity. We assume that all of the electrons are swept out and that all of the holes are very quickly trapped near the interface. Tending to balance the trapping of holes is recombination with electrons, which we take to be proportional to the trapped hole concentration, P_t cm^{-2}, and the free electron density, n cm^{-3}. Then we can write

$$\frac{dP_t}{dt} = \frac{\alpha d_o J_{FN}}{q} - R\, P_t\, n \tag{6-5}$$

where R is a recombination-rate constant of proportionality. We write the density of electrons as

$$n = \frac{J_{FN}}{\mu_n\, q\mathcal{E}}$$

where μ_n is the mobility of electrons in the SiO_2. Equation (6-5) can be rewritten as

$$\frac{dP_t}{dt} = \frac{\alpha d_o J_{FN}}{q} - R\, P_t \left(\frac{J_{FN}}{\mu_1\, q\mathcal{E}}\right) \tag{6-6}$$

Assume that the holes are trapped near the tunneling contact. Then in Eq. (6-4) we can set x approximately equal to d_o and write

$$\int_o^{d_o} \rho(x)dx = q\, P_t \ .$$

Equation (6-4) can now be rewritten as

$$\mathcal{E}_c = \frac{V_a}{d_o} + \frac{P_t(t)\, q}{\varepsilon} \tag{6-7}$$

The effect of the enhancement of electric field near the tunneling contact can be shown by replacing $\mathcal{E}$ with $\mathcal{E}_\xi$ in Eq. (6-2), neglecting the effect on the pre-exponential term $C\mathcal{E}^2$. Then we have

$$J_{FN} = C\mathcal{E}^2 \exp\{-\mathcal{E}_o/[V_a/d_o + P_t(t)\ q/\varepsilon]\} \tag{6-8}$$

Since there is no simple analytical solutions for these two simultaneous equations, (6-6) and (6-8), the straightforward way to find P(t) and the value of α is to deduce them directly from the experimentally obtained time-dependent current (such as is shown in Fig. 6-5(a)).

Suppose that $P_t(t = 0) = 0$. Then we can write from Eq. (6-8):

$$I(t)/I(t=0) = J_{FN}(t)/J_{FN}(t=0)$$

$$= \exp\{-\mathcal{E}_o/[V_a/d_o + P_t(t)\ q/\varepsilon]\}/\exp(-\mathcal{E}_o\ d_o/V_a)\ .$$

Solving this expression for $P_t(t)$ in terms of $I(t)/I(t=0)$ results in:

$$P_t(t) = (\varepsilon/q)\{\mathcal{E}_o/(\mathcal{E}_o d_o/V_a) - \ln\ [I(t)/I(t=0)]\} - (\varepsilon/q)(V_a/d_o) \tag{6-9}$$

From this relationship $P_t(t)$ can be plotted point by point since $I(t)/I(t=0)$ is known. The result for $P_t(t)$ is shown in Fig. 6-10 for V_a = 195V.

From Eq. (6-6) we obtain for the initial value of $d\ P_t(t)/dt$:

$$\left.\frac{d\ P_t(t)}{dt}\right|_{t\sim o} \simeq \left.\frac{\alpha d_o J_{FN}}{q}\right|_{t\sim o} \tag{6-10}$$

The initial slope of $P_t(t)$ can be determined from Fig. (6-10). The resulting value of αd_o is estimated to be 7-8 x 10^{-4}. This value of αd_o is small enough that the additional electrons supplied by multiplication $\alpha d_o J_{FN}$ can be neglected in the total current, and the main factor causing the current instability is the positive feedback

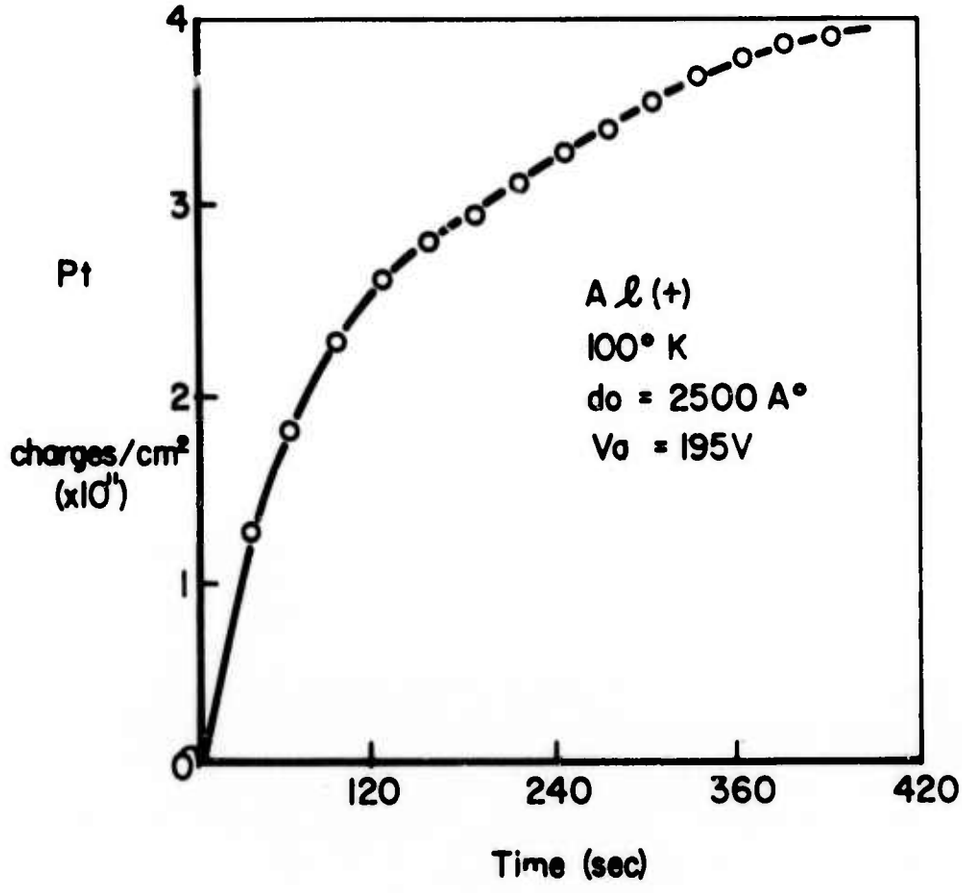

Fig. 6-10 The positive charge density plotted as a function of time, deduced from current-time curve for V_a = 195V in Fig. 6-5(a).

caused by the accumulation of holes near the interface. The quantity α is undoubtedly a function of electric field intensity and sample temperature.

Because the current instability is reproducible and the current is proportional to the area of the field plate, the impact process presumably occurs over the entire sample. However, localized breakdown will take place when momentarily a microscopically unbalanced situation between impact ionization and recombination occurs locally due to local defects or simply statistical fluctuations of the impact process. If we assume that under this condition the generation and trapping of holes locally overcomes recombination, we can write Eq. (6-5) approximately as

$$\frac{d P_t}{dt} = \frac{\alpha d_o J_{FN}}{q} \tag{6-11}$$

Then

$$J_{FN} = C\mathcal{E}^2 \exp\{-\mathcal{E}_o/[V_a/d_o + \int_o^t (\alpha d_o J_{FN}/\varepsilon)dt]\} \tag{6-12}$$

Equation (6-12) will show the differential negative resistance region needed to explain the breakdown switching process shown in Fig. (1-2).

Based on this breakdown model, the local current filament still consists of electron current only. This matches the hypothesis, mentioned in Chapter IV, that the breakdown filament has essentially an electron current. Because of the presence of low-mobility holes in SiO_2, the electron current will not be space-charge limited in spite of their high current density on breakdown.

VI-5 Temperature-Dependent and Substrate-Dependent C-V Curves After High Field Stress

The first effect of high field stress on C-V curves of Al-SiO_2-Si structure is the increase of interface states. However, the increase of interface states usually is not high enough to contribute

much smear-out to the C-V curves.

If the current instability is observed in high fields, the C-V curves measured afterwards do show some temperature-dependence.

To illustrate this dependence, Figs. 6-11(a) and (b) show two sets of C-V curves corresponding to samples of both p-type and n-type substrates. At 100°K, in both figures, the C-V curves shown with dashed lines shift toward negative bias almost parallel to the original one after the current instability is seen. After the samples are warmed up to room temperature (with either open-circuit contact or short-circuit contact) the C-V curves change from the dashed lines to those drawn with solid lines - the C-V curves show more smear-out. If the samples are cooled again, the C-V curves do not return to those shown by dashed lines, but retains a smear-out. This irreversible change is found to be associated with temperature only, because the parallel-shifted C-V curves can be "frozen" at 100°K for several hours without any significant smear-out and if the sample is warmed up in ten minutes, the smear-out will appear.

The parallel shift in C-V curves can only be obtained when the current instability is produced at low sample temperatures (say, 100°K). If the high field is applied at room temperature and the current instability is seen, the C-V curves will have the same shape as those shown by the solid lines in Figs. 6-11(a) and (b). The flatband shift at room temperature is greater with p-type substrates than with n-type substrates. The interface states are found to increase from about 5×10^9 states/cm^2 on a fresh sample to 2×10^{10} states/cm^2 on a sample after stress as determined by G-V measurements at room temperature.[33] This density of interface states alone cannot account for the almost 10 volt smear-out in the C-V curves, and a nonuniform distribution of positive space charges in the oxide ought to be considered. However, the reason why the positive space charge cannot maintain its uniform distribution from 100°K to 300°K is not clear.

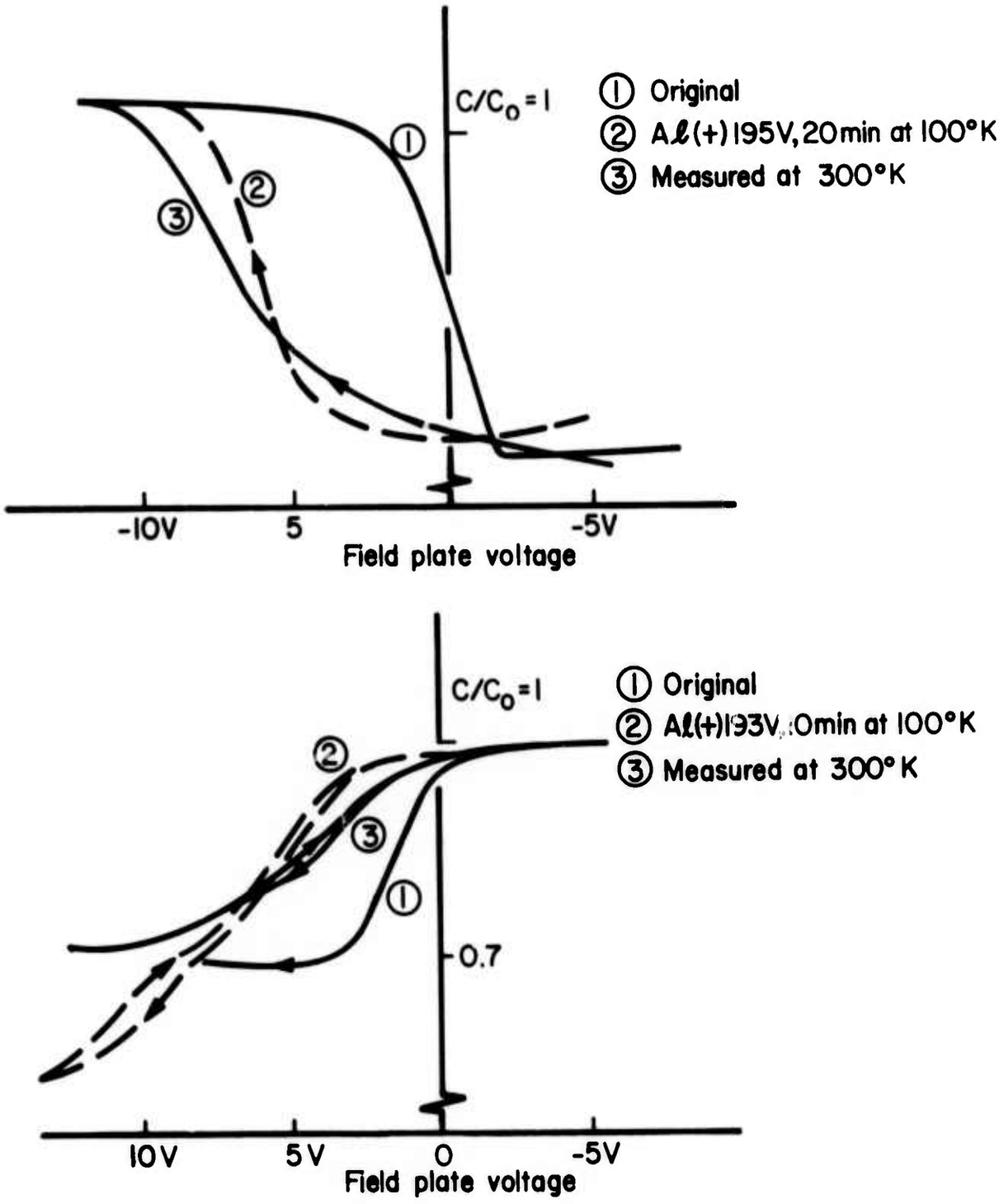

Fig. 6-11 Temperature-dependent and substrate-dependent C-V curves after high field instability. (a) on p-type substrate (b) on n-type substrate.

No matter what the actual reason is for the large smear-out in C-V curves at room temperature and the irreversible change in C-V curves with temperature, the smear-out does impose difficulties in comparing the generation of positive charges in high field at different temperatures.

VI-6 Summary and Discussion

In this chapter, a series of experiments are described which attempt to identify the actual mechanism of breakdown initiation.

First, the current conduction is confirmed to be due to electron tunneling from negatively-biased contact in SiO_2 following the Fowler-Nordheim equation. By comparing the theoretical equation and the experimental result, the effect mass is found to be 0.38 m_o for electron tunneling from Si and 0.46 m_o for electron tunneling from an Al field plate.

A current instability is found at very high fields and can be associated with positive space charge in the SiO_2. The current instability is found at lowered temperature as well as at room temperature.

A model using impact ionization and the trapping of holes is used to explain the current instability and the breakdown mechanism.

In comparing the theoretical model and experimental data, the impact coefficient is found to be around 10^{-3} at field intensities approaching breakdown of the SiO_2 - a fairly small value.

Finally, the observed temperature-dependence and substrate-dependence of C-V curves after current instability are presented but have not yet been explained satisfactorily.

Though the model presented here is sufficient to expalin the observed experimental results, there are several points to be discussed:

(1) Although impact ionization has previously been suggested as the principal process to account for the dielectric breakdown of SiO_2, the present study was the first, to our knowledge, to establish the fact that positive charges are actually generated and stored in SiO_2 after

the presence of a pre-breakdown current instability. We have shown experimentally the dependence of this instability on temperature and have explained the instability on the basis of the generation and trapping of holes. O'Dwyer[34] has made a detailed analysis of a similar model, but he neglected recombination.

Since the impact coefficient is about 10^{-3}, the major effect of the impact ionization comes from the positive space charge of holes which are trapped near the tunneling contact and which exert great effect on the tunneling current. Recently, Klein and Solomon,[35] using internal photoemission, reported that current multiplication has been observed in Al_2O_3 but not in SiO_2. Although they suggested that there may not be impact ionization in SiO_2, their argument may not be conclusive if the impact coefficient is as small as 10^{-3} at field close to 7.8×10^6 V/cm. However this low impact coefficient can result in a major effect through hole trapping and the sensitive field-dependence of the tunneling current.

(2) Whether a significant fraction of electrons in amorphous SiO_2 can gain such a high kinetic energy as 9eV is still controversial. However, hot electrons in other amorphous insulators have been reported previously. The current multiplication in Al_2O_3 observed by Klein and Solomon[35] shows that hot electrons do exist in Al_2O_3 and are able to produce impact ionization. Hot electrons have also been detected in SiO_2 by using a metal-oxide-metal structure in which electrons are injected into the oxide in high fields and gain enough energy to escape, without much attenuation in the thin anode, into vacuum where they are collected.[35] The thickness of the SiO can be of several thousand Å. In our experiments on SiO_2, the low value of impact coefficient ($\alpha \sim 10^{-3}$) can be interpreted to mean that only a small fraction of electrons in the SiO_2 have gained a large kinetic energy.

(3) The difference in breakdown field strengths with opposite applied field polarities may arise, at least in part, from the difference in distributions of hole trapping centers near the two interfaces.

(4) Our model does not, in itself, explain the scratch effect mentioned in Chapter IV-1(c). Why the scratches on Al field plate affect only the positive field-plate-polarity breakdown may be caused by field enhancement around the field-plate scratches which makes hole tunneling into the SiO_2 possible, resulting in a double-injection type current filament.[37] However, if the scratched field plate is biased negatively, the local high field only enhances the electron tunneling. The positive charges, which are essential to the positive feedback, are still controlled by impact ionization in the bulk. The impact ionization coefficient presumably depends only on the magnitude of the field and on the temperature, and not on the magnitude of the tunneling current. Therefore, although the scratches enhance the tunneling current, they are not able to cause nucleation of field-plate-negative breakdows at lower fields.

CHAPTER VII
CONCLUSIONS

In this work we have used the non-shorting self-quenched breakdown technique to study the initiation of localized breakdown, the breakdown discharge process, and the final damage topography.

In the study of the mechanism of breakdown initiation, the experimental results indicate that the conduction starts with Fowler-Nordheim electron tunneling. In the pre-breakdown region a current instability is observed and is found to be closely associated with the presence of a positive stored charge. Further, the current instability is found to be dependent on the temperature. The conclusion drawn from these results is that the breakdown is probably initiated by an impact ionization process in the SiO_2; the positive charges are holes which are created by the impact ionization process and are trapped near the tunneling contact where they enhance the tunneling current. In our experiment at 100°K on 2500Å thermally grown SiO_2 films, we would the ratio of the holes generated to electrons injected to be of the order of 10^{-3} in the pre-breakdown unstable regime.

The breakdown process is believed to result from a microscopically unbalanced positive feedback in which a local buildup of positive charge results in runaway of the electron tunneling contact. The switching process from a low-current high-voltage state to a high-current low-voltage state is the result of the formation of a current filament through which the MOS capacitor discharges its stored energy.

The breakdown discharge study reveals that on the occurrence of breakdown, the current filament contributes only a negligible electrical resistance, comapred with that contributed by the silicon substrate, to the discharge current. Therefore most of the dissipation of stored electrical energy into heat occurs in the silicon rather than in the SiO_2 itself. Hence the current-density pattern in the silicon substrate will determine the heat-generation

pattern and consequently determine the topography of the local breakdown damage.

Experimentally, the topographical structures of self-quenched breakdowns, as shown in optical and SEM micrographs, are found to be distinct among the four combinations of applied-voltage polarity and substrate type. The differences and similarities can be correlated with the field plate polarity and the conduction regime of the substrate, i.e., inversion or accumulation. The differences in topographical appearance can be explained on the basis of different discharging current-density patterns in the substrate during the breakdown discharge process.

Square self-quenched breakdown was first observed in this study on (100) p-type silicon substrate wafers with positive field-plate polarity. This anisotropic breakdown pattern can be interpreted as the result of anisotropic conductivity of hot electrons in the n-inversion layer after the occurrence of breakdown. Based on this interpretation and the properties of the anisotropic conductivity, it was predicated that the breakdown pattern on this particular configuration should evolve from round to square and then to stellar shape as the breakdown voltage increased. Upon using a thick oxide to increase the breakdown voltage, the predication was confirmed.

REFERENCES

1. H. Sträb and H. Maylandt, "Present Stage of the Technique of Metallized Paper Capacitor for Power System," 1958 Conf. Int. des Grands Ré-seaux Electriques, Paris, Rept. 109.
2. N. Klein and H. Hafni, "The Maximum Dielectric Strength of Thin Silicon Oxide Films," IEEE Trans. Electron Devices ED-13, 281 (1966).
3. N. Klein, "The Mechanism of Self-Healing Electrical Breakdown in MOS Structure," IEEE Trans. Electrod Devices ED-13, 788, (1966).
4. S. Whitehead, "Dielectric Breakdown of Solids," Oxford Univ. Press, London and New York, 1953.
5. J. J. O'Dwyer, "The Theory of Dielectric Breakdown of Solids," Oxford Univ. Press, London and New York, 1964.
6. N. Klein, "Electric Breakdown in Solids," Advances in Electronics and Electron Physics, 26, Academic Press, New York (1969).
7. P. J. Harrop and D. S. Cambell, "Dielectric Properties of Thin Films," Handbook of Thin Film Technology, Chap. 16, McGraw Hill, New York (1970).
8. N. Klein and N. Levanon, "AC Electrical Breakdown in Thin Silicon Oxide Films," J. Appl. Phys. 38, 3721 (1967).
9. B. P. Budenstein and P. J. Hayes, "Breakdown Conduction in Al-SiO-Al Capacitors," J. Appl. Phys. 38, 2837 (1967).
10. F. L. Worthing, "D-C Dielectric Breakdown of Amorphous Silicon Dioxide Films at Room Temperature," J. Electrochem. Soc. 115, 88 (1968).
11. M. Lenzlinger and E. H. Snow, "Fowler-Nordheim Tunneling into Thermally Grown SiO_2," J. Appl. Phys., 40, 278 (1969).
12. P. Wang, N. Van Buren and P. Edraos, "SEM Observation of Self-Healing Breakdown in Thermally Grown SiO_2 Films," J. Electrochem. Soc. 117, 127 (1970).
13. N. J. Chou and J. M. Eldridge, "Effects of Material and Processing Parameters on the Dielectric Strength of Thermally Grown SiO_2 Films," J. Electrochem. Soc. 117, 1287 (1970).

14. C. M. Osburn and D. W. Ormand, "Dielectric Breakdown in Silicon Dioxide Films on Silicon, Parts I and II," J. Electrochem. Soc. 119, 591 (1972).

15. C. M. Osburn and E. J. Weitzman, "Electrical Conduction and Dielectric Breakdown of Silicon Dioxide Films on Silicon," J. Electrochem. Soc., 119, 603 (1972).

16. M. Shatzkes, M. Av-Ron and R. M. Anderson, "On the Nature of Conduction and Switching in SiO_2," J. Appl. Phys. 45, 2065 (1974).

17. J. W. Davisson, "The Orientation of Electrical Breakdown Path in Single Crystals," Phys. Rev. 70, 685 (1946).

18. E. L. Offenbacher and H. B. Callen, "Directional Effects in the Electric Breakdown of Ionic Crystals," Phys. Rev. 90, 683 (1953).

19. R. Cooper and C. T. Elliott, "Directional Electric Breakdown of KCl Single Crystals," Brit. J. Appl. Phys. 1, 121 (1968).

20. G. G. Harman, "Topological Features of Hot Carrier Induced Anisotropic Breakdown on Silicon Diode Surfaces," Jour. Res. NBS, 73A, 321 (1969).

21(a). M. Shibuya, "Hot Electron Problems in Semiconductors with Spheroidal Energy Surfaces," Phys. Rev. 99, 1189 (1955).

(b). W. Sasaki, M. Shibuya, "Experimental Evidence of the Anisotropy of Hot Electrons in n-type Germanium," J. Phys. Soc. Japan 11, 1202 (1956).

(c). W. Sasaki, M. Shibuya, and K. Mizuguchi, "Anisotropy of Hot Electrons in n-type Germanium," J. Phys. Soc. Japan 13, 456 (1958).

22. E. Conwell, High Field Transport in Semiconductors, Chap. II, Academic Press (1967).

23. R. A. Smith, Wave Mechanics of Crystalline Solids, Chap. 5, Chapman and Hall, London (1969).

24. W. E. K. Gibbs, "Conductivity Anisotropy and Hot Electron Temperature in Silicon," J. Phys. Chem. Solids 25, 247 (1964).

25. M. Asche, B. L. Boitschenko and O. G. Sarbej, "Abhängigkeit der Anisotropie der Elektrischen Leitfähigkeit des Siliziums vom Elektrischen Feld," Phys. Stat. Sol. 9, 323 (1965).

26. C. Canali, G. Ottaviani and A. Albeigi Quaranta, "Drift Velocity of Electrons and Holes and Associated Anisotropic Effects in Silicon," J. Phys. Chem. Solids 32, 1707 (1971).

27. Z. Weinberg, Ph.D. Thesis, Princeton University (1974).

28. E. Burgess, H. Kroemer and J. M. Houston, "Corrected Values of F-N Field Emission," Phys. Rev. 90, 515 (1953).

29. T. H. DiStefano and D. E. Eastman, "Photoemission Measurement of the Valence Level of Amorphous SiO_2," Phys. Rev. Lett. 27, 1560 (1971).

30. A. M. Goodman, "Electron Hall Effect in Silicon Dioxide," Phys. Rev. 164, 1145 (1967).

31. R. Williams, "Photoemission of Electrons from Silicon into Silicon Dioxide," Phys. Rev. 140, A569 (1965).

32. T. H. DiStefano and D. E. Eastman, "The Band Edge of Amorphous SiO_2 by Photoinjections and Photoconductivity Measurements," Sol. State Comm. 9, 2259 (1971).

33. C. C. Chang, private communication.

34. J. J. O'Dwyer, "Theory of High Field Conduction in a Dielectric," J. Appl. Phys. 40, 3887 (1969).

35. N. Klein and P. Solomon (to be published).

36. R. A. Collins and R. D. Gould, "Hot Electron Transport and Emission and Au-SiO-Au Thin Film Cathodes," Solid State Elect. 14, 805 (1971).

37. M. A. Lampert and P. Mark, Current Injection in Solids, Chap. 14, Academic Press, New York (1970).